



Examining Multidecadal Variations in Glacier Surface Temperature at Debris-Covered Alamkouh Glacier in Iran (1985–2020) Using the Landsat Surface Temperature Product

Neamat Karimi¹ · Omid Torabi¹ · Amirhossein Sarbazvatan¹ · Sara Sheshangosht¹

Received: 28 April 2023 / Accepted: 12 December 2023

© Deutsche Gesellschaft für Photogrammetrie, Fernerkundung und Geoinformation (DGPF) e.V. 2024

Abstract

This study aimed to assess the temporal changes in glacier surface temperature (GST) for the debris-covered Alamkouh glacier (over 88% of the total glacier area is debris covered), located in Iran, over the period from 1985 to 2020. The analysis employed the Landsat surface temperature product at a spatial resolution of 30m. The research pursued three primary objectives: (1) a spatiotemporal analysis of GST changes, (2) an evaluation of correlations between GST and glacier variables such as ice-thickness change and albedo, and (3) the identification of factors influencing GST, including air temperature, cloud cover, precipitation, and snowfall, utilizing the Global Land Data Assimilation System dataset. Spatial changes were analyzed using the Mann–Kendall trend test and Sen’s slope estimator, revealing statistically significant positive or negative trends in all multitemporal parameters. The spatial change analysis showed that GST increased between 0 and +0.2 °C/a from 1985 to 2020. The mean annual GST increase for the entire glacier is 0.086 °C/a, signifying a 3 °C rise over 36 years. High-altitude regions exhibit more substantial GST increases than lower-altitude areas do, although a discernible pattern across the glacier’s surface remains elusive. To complement the spatial GST analysis, we divided the study period into four periods, 1985–1990, 1990–2000, 2000–2010, and 2010–2020, and mean GST was calculated separately for ablation months. Results indicate stability in mean GST from 1985–1990 to 1990–2000, followed by a significant increase of 2.3 °C/decade from 1990–2000 to 2000–2010, representing the largest increase observed. Temporal change analysis over 36 years reveals that the most significant warming occurs in debris-covered areas (0.139 °C/a), with less warming observed in debris-free regions (0.097 °C/a) during both accumulation and ablation months. The study employed the normalized difference snow index to identify debris-free areas and assess their potential impact on GST. First, the results establish a robust inverse relationship between GST and the extent of debris-free terrain. Second, the analysis demonstrates a significant reduction in debris-free terrain at a rate of –0.035% per month since 1985, culminating in a 15.12% decline over 36 years, encompassing both accumulation and ablation periods. Additionally, outcomes from the albedo analysis reveal a robust negative correlation between albedo and mean GST, with an R^2 of 0.57. The examination of albedo alterations shows a substantial annual decrease of approximately –0.08/a across the entirety of the glacier terrain, while albedo remains stable in low-elevation areas over the 36-year period, with significant changes occurring in high-elevation debris-free regions. In contrast, a comprehensive examination reveals that a robust association between the glacier ice-thinning rate and GST change cannot be ascertained. Among climate variables, air temperature exhibits significant warming, increasing at a rate of 0.016 °C/a from 1985 to 2020, while other variables remain stable. Understanding these multifaceted influences on glacier surface temperature is vital for adapting to ongoing climate changes in glacial regions. Further research is needed to disentangle intricate interactions among climate parameters and their cumulative effects on glacier dynamics.

Keywords Glacier Surface Temperature (GST) · Debris-covered Glacier · Temporal Changes · Spatial Analysis · Climate Variable

✉ Neamat Karimi
n.karimi@wri.ac.ir

¹ Department of Water Resources Study and Research, Water Research Institute, Tehran, Iran

1 Introduction

A change in climate is well reflected in the state of glaciers as well as in their mass balance, and so these are recognized as being reliable indicators of global warming and climatic change (Liao et al. 2020; Zemp et al. 2015). Glacier length, area, volume, and mass balance changes contribute to sea level rise, impact the regional water cycle, and may trigger surges and glacier lake outburst floods (Chudley et al. 2017; Gardelle et al. 2013; Hartl et al. 2020; Lovell et al. 2018; Watson et al. 2020; Yan et al. 2017). As a consequence, long-term monitoring of the past, present, and future glacial features and processes is essential for the assessment of land management and policymaking in relation to environmental systems (Gärtner-Roer et al. 2019; Karpilo Jr. 2009).

Alpine glaciers, which are found in rugged and remote mountainous areas, pose challenges for researchers and scientists due to their difficult accessibility (Brun et al. 2017). This difficulty hinders the study, monitoring, and conservation of these glaciers and leaves them susceptible to various threats, including human activities and climate change (Robson et al. 2021). Field measurements in glacial areas are labor intensive and challenging (Cao et al. 2021), making remote sensing approaches essential for studying glaciers and analyzing their changes over time (Dehecq et al. 2019; Muhammad and Tian 2020; Wu et al. 2020). Remote sensing technologies can provide spatially quantitative and qualitative datasets to measure glacier change rates, especially in the context of our warming climate (Hauser and Schmitt 2021; Pellikka and Rees 2010). It is important to note that both remote sensing and field work are complementary approaches with distinct advantages and limitations in glacier studies.

Among all glacial features and processes, glacier surface temperature (GST) is one of the most important parameters because it influences various processes within and around glaciers. Monitoring and studying GST are vital components of climate research, glacier monitoring, and environmental assessments, with implications for both scientific understanding and societal concerns related to climate change and glacier-dependent regions (Anul Haq et al. 2012; Hall et al. 2008; Wu et al. 2015). Glacier surface temperature, which is called the superficial temperature of the glacier surface, is the temperature that is measured at the surface of a glacier, and it is a direct reflection of the energy balance at the glacier surface (Wu et al. 2015). It is correlated with the negative or positive mass balance of the glacier (Liao et al. 2020; Yalcin and Polat 2020); GST is remarkably sensitive to the processes related to both glacier situation (e.g., thermal dynamics at the ice, snow, debris, and water surfaces) and climatic conditions (e.g., increasing or decreasing air temperature, cloud cover, and

any other parameters that change the energy flux from the atmosphere, such as humidity, aerosols, and fog).

Existing research suggests that the presence of debris components on the surfaces of glaciers poses challenges in accurately assessing and comprehending the impacts of climate change on these icy formations (Bhardwaj et al. 2014). This is due to the accumulation of debris acting as a confounding variable that obstructs the unambiguous examination of the dynamic relationship between climate change and glacial behavior. However, apart from enabling the identification and delineation of debris-covered actual glacier areas (Alifu et al. 2020; Tarca and Guglielmin 2022), surface temperature data also offer opportunities to evaluate the effects of climate change. In fact, surface temperature has a critical role in regulating the heat budget and controlling the extent of ice loss on debris-covered glaciers. Therefore, comprehending surface temperature is essential for simulating the evolution of such glaciers and their response to climate changes (Wu et al. 2015). In this context, surface temperature measurements can be utilized in energy balance modeling (Rounce et al. 2020) to estimate the amount of ice loss on glaciers, and these outcomes can be further integrated into mass balance models (Azam and Srivastava 2020; Vincent et al. 2005).

To date, there have been only a few studies conducted on the GST of glaciers (Hall et al. 2008; Lo Vecchio et al. 2018a; Wu et al. 2019, 2015). In addition, research on the temporal evolution of GST on debris-covered alpine glaciers is scarce, and there has been limited exploration of the spatiotemporal variations of GST. Furthermore, in some limited studies, only a few images were used, and accurate spatiotemporal GST changes of glaciers are hard to obtain. It is essential to emphasize that one of the greatest challenges in this field has a lot to do with the lack of ground-based data from which satellite-based data can be calibrated and validated over glacial areas. A limited number of studies have been conducted in this area, with Liao and colleagues' study in 2020 being one of the most prominent. In this study, multitemporal Landsat 5 and 8 images were used to investigate the GST change of Hailuoguo glacier in the Tibetan plateau from 1990 to 2018. Using a mono-window algorithm for GST calculation, the authors found that the GST of this glacier showed a low increasing trend at a rate of 0.054 °C/a (Liao et al. 2020).

The primary objective of the present study was to investigate the alterations in GST from 1985 to 2020. This was accomplished by employing thermal bands derived from satellite imaging data obtained from Landsat 5, 7, and 8. The region of interest for this investigation was the Alamkouh glacier situated in Iran. The study encompassed three key aims, each of which will contribute to advancing our comprehension of GST transformations in Iran. First, the temporal and spatial analysis involved assessing variations

in GST gradients and GST anomalies across both debris-free and debris-covered glacier surfaces. This assessment will provide insights into the intricate spatial dynamics of GST alterations.

Second, the investigation evaluated the relationship between GST variations and other significant factors associated with glacier changes. These factors include glacier ice-thinning rate and glacier albedo. By examining these interconnections, a more comprehensive understanding of the complex interactions between GST and other glacier characteristics can be established.

Lastly, the research was designed to identify and evaluate the meteorological factors and mechanisms contributing to alterations in GST (including air temperature, cloud cover, precipitation, and snowfall).

2 Study Area

The Alamkouh glacier (36° 23.50' N, 50° 58.62' E) is located in the north of Iran on the western side of the Alburz mountain (Fig. 1). The area of this glacier is about 3.8 km², and the elevation ranges from 3623 to 4405 m above sea level (Karimi et al. 2012b). The Alamkouh glacier had not been studied for GST analysis previously, and the majority of studies have focused on identifying the glacier area (Moussavi et al. 2009), evaluating the change in surface area (Farajzadeh and Karimi 2014; Karimi et al. 2014), or analyzing the change in ice thickness (Karimi et al. 2012b). Results of the latest analysis performed on glacier inventory in this region indicated that over 88% of the glacier area is debris covered, and only 12% of the glacier area is debris free (Karimi et al. 2012a). According to the study conducted by Karimi et al. (2022), the mean annual surface velocity of the Alamkouh glacier was approximately 1 m/a. Furthermore, their previous research (Karimi et al. 2021b) revealed that the mean rate of ice thinning experienced by the glacier between 2018 and 2020 was estimated to be around -0.23 ± 0.03 m/a, with the maximum thinning rate about -5 ± 0.65 m/a at the debris-free areas.

The Alamkouh glacier exhibits a unique combination of features observed in both debris-covered glaciers and rock glaciers. Flow unit 1, which represents the debris-covered glacier component, is characterized by a relatively small accumulation area, the presence of some small supraglacial lakes, a substantial ice thickness of 38 m, a considerable rate of elevation change (-0.37 m/a), and a relatively high surface velocity of 1.3 m/a. In contrast, flow units 2 and 3 display characteristics typical of rock glaciers. These include the presence of multiple flow lobes; a scarcity of clean ice; the absence of supraglacial lakes; a thinner ice thickness, with flow unit 2 measuring 26 m and flow unit 3 measuring 17 m; a very low velocity of approximately 0.3 m/a; and an

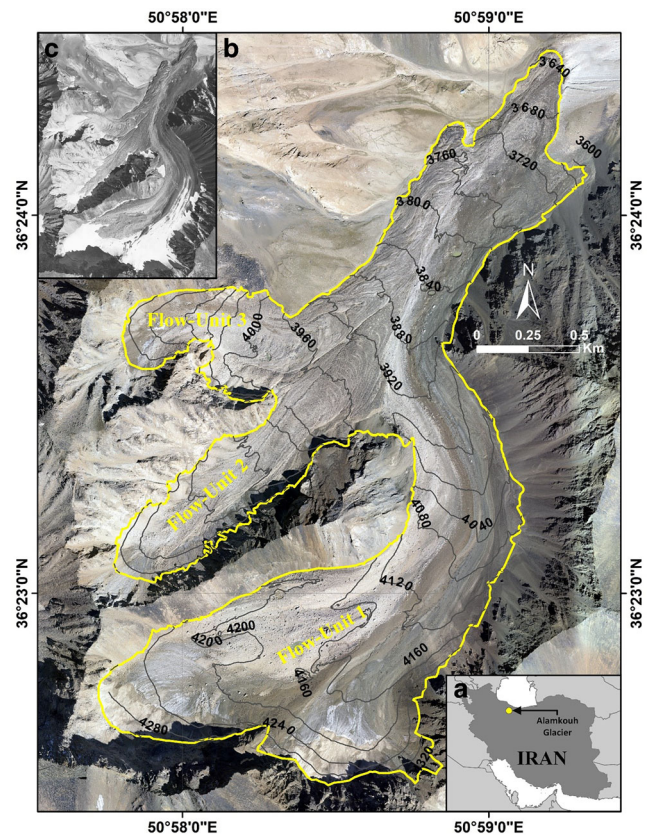


Fig. 1 a Location map of Alamkouh glacier in Iran. b Overview of the Alamkouh glacier surface (aerial photo acquired in September 2020). The yellow line on the map indicates the current extent of the glacier based on the latest glacier inventory in 2020 using unmanned aerial vehicle high-resolution aerial photography. c A historical condition of the glacier (aerial photo acquired in September 1955)

almost negligible thinning rate that approaches zero. The juxtaposition of these distinct flow units within the Alamkouh glacier highlights the hybrid nature of this glacier. While flow unit 1 displays traits more commonly associated with debris-covered glaciers, flow units 2 and 3 exhibit properties akin to rock glaciers (Karimi et al. 2022, 2021b). This unique combination underscores the need for further investigation and analysis to better comprehend the mechanisms driving the glacier change.

3 Data and Methodology

3.1 Landsat Surface Temperature Product

Various methods for calculating land surface temperature using remote sensing data have been explored, including mono-window, split-window, and multichannel techniques (Liao et al. 2020; Qin et al. 2001; Sattari and Hashim 2014). These methods have applications across different land and sea surfaces but have both advantages and draw-

backs. Key parameters for accurate LST calculation include surface emissivity, atmospheric transmittance (water vapor), and effective mean air temperature, which are determined using various empirical models and meteorological data (Jiménez-Munoz and Sobrino 2003; Kane et al. 2016; Sobrino et al. 1991; Zhang et al. 2017). As a consequence, GST can be calculated using raw satellite images only if several types of meteorological and ancillary data are available near the glacial regions, which is not always possible due to glaciers' remoteness. It is more of an issue in Iran, and it is glacial areas, as there are very little meteorological data available locally in these regions, that are of specific concern for accurate GST measurement. On the other hand, satellite-based meteorological data could not be used in this study due to their low spatial resolutions and short-time datasets. Hence, in this study, a prepared product of LST was employed in order to investigate how the surface temperature of the Alamkouh glacier changes in response to global climate change.

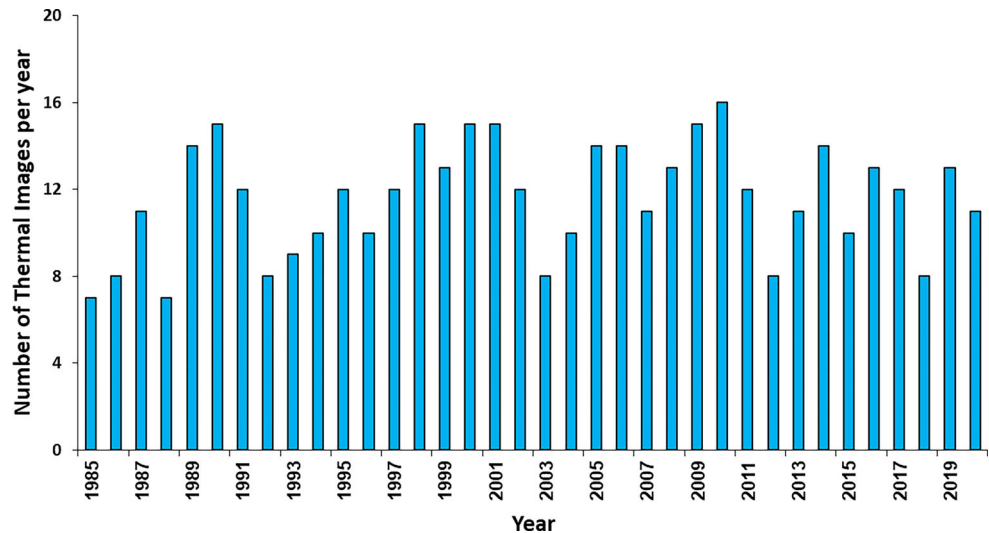
In the present study, Landsat Collection 2 Level 2 surface temperature science products (L2SP; Cook et al. 2014) were used for GST variability analysis over the study area. These data were produced using the Landsat surface temperature algorithm (version 1.3.0) developed in partnership with the Rochester Institute of Technology (Rochester, NY, USA) and the NASA Jet Propulsion Laboratory (Pasadena, CA, USA) for all Landsat thermal bands; the data were produced from the Landsat Collection 2 Level 1 thermal bands, top of atmosphere surface reflectance, top of atmosphere brightness temperature, ASTER Global Emissivity Database, ASTER normalized difference vegetation index (NDVI), and atmospheric profiles of geopotential height, specific humidity, and air temperature extracted from the GEOS version 5 Forward Processing Instrument Teams model (for Landsat images from 2000 to present) or the Modern Era Retrospective Analysis for Research and Applications version 2 (for Landsat images from 1982 to 1999; Cook et al. 2014).

It is important to note that the accuracy of the L2SP products may be improved by using ground-based measurements for validation and calibration purposes. Additionally, users should carefully evaluate the quality assessment and uncertainty information provided with the L2SP products before using them for scientific research or decision-making purposes. However, it is of paramount importance to consider the difficulty of evaluating the surface temperature products using ground data in our glaciated region as a reference point. In our research area, it is virtually impossible to acquire ground data, particularly when a satellite is traversing the region, making it highly arduous and practically unfeasible to obtain ground data. This concern is frequently beset by challenges stemming from the formidable inaccessibility of mountainous and glacial terrains on one

hand and the prevalent cloud cover enshrouding a considerable number of satellite depictions on the other hand. Conversely, there are a number of elements that complicate the task, such as the distinction between in situ observations, which are simply point measurements, and satellite-derived observations, which are indicative of a significantly larger region (Hall et al. 2008). Therefore, we are unable to assess the precision of the L2SP product. This is a common predicament in glaciology studies that must be addressed, and in many analogous studies that have utilized GST measurements for glacier surface temperature assessment, in situ measurements have not been employed (Anul Haq et al. 2012; Liao et al. 2020; Lo Vecchio et al. 2018b; Wu et al. 2019; Yalcin and Polat 2020). Several studies have evaluated the accuracy of Landsat surface temperature products, including the L2SP products over nonglacial areas. These studies have shown that the accuracy of the surface temperature measurements can vary depending on the conditions and land covers, but they typically have an accuracy of $\pm 1-2^{\circ}\text{C}$ (Cook et al. 2014; Laraby and Schott 2018; Malakar et al. 2018; Schaeffer et al. 2018). For example, the L2SP product, encompassing data from Landsat 5, 7, and 8 satellites, has recently undergone rigorous evaluation within the contiguous United States over the 2009–2019 period (Duan et al. 2021). This examination leveraged in situ measurements obtained from 21 distinct monitoring sites. The outcomes of this study revealed the attainment of a notable degree of consistency in the performance of the L2SP product across a significant portion of the examined sites. It is important to note, however, that certain vegetated locations exhibited substantial discrepancies characterized by significant bias and root mean square error (RMSE). Importantly, when considering surfaces subject to snow cover, the mean bias and RMSE, representing the disparities between the L2SP product and in situ measurements, approximated -1.1 and 1.6 K, respectively. It should be noted that the accuracy of LST products may be higher or lower depending on the specific conditions of the study area.

An extensive analysis of all Landsat satellite images taken since 1985 was conducted in order to eliminate any images that contained cloud cover over the research area. As a result, a total of 428 images spanning 36 years from 1985 to 2020 were identified and utilized to calculate the GST of the Alamkouh glacier. This compilation included 211 Landsat-5 Thematic Mapper (TM) images from 1985 to 2011, 117 Landsat-7 Enhanced Thematic Mapper Plus (ETM+) images from 2000 to 2012, and 100 Landsat-8 Thermal Infrared Sensor (TIRS) images from 2013 to 2020. Among the series of Landsat satellite images, the TIR signal measured by Landsat 5 has the highest weight, around $12\mu\text{m}$, followed by Landsat 7 and 4. Since water vapor absorption/emission in the $12\text{-}\mu\text{m}$ spectral region is higher than in the $10\text{-}11\text{-}\mu\text{m}$ region, a larger contribution from

Fig. 2 Number of thermal images used per year for analysis of glacier surface temperature changes across the Alankouh glacier



the 12- μm region decreases the algorithm’s retrieval performance (Ermida et al. 2020). The TIR band of Landsat 8 is considerably narrower than for the other Landsats and excludes the 12- μm region, which contributes to an enhanced precision in retrieving LST.

Figure 2 displays the frequency at which surface temperature products were employed in all years during the study period. It was determined that the number of images fluctuated depending on the presence of cloud cover, ranging from a minimum of seven images in 1988 to a maximum of 16 images in 2010. In order to ensure that the monthly data were consistent, averaging was performed when there were multiple images in a month. In some limited cases, data from the previous and following years were used when there was not an image in a certain month, especially due to the cloud cover in satellite images acquired during the fall and winter seasons.

3.2 Glacier Albedo Calculation Using Landsat Optical Bands

Glacier albedo refers to the reflectivity of the glacier’s surface. It is defined as the ratio of the reflected radiant flux from the glacier surface to the incident radiant flux over the solar spectrum (Wu et al. 2023). Albedo and GST are often involved in a feedback loop. When GST increases due to various factors such as climate warming, it can lead to changes in glacier surface properties. Higher GST can accelerate the melting of ice and snow, reducing the glacier’s surface albedo as it exposes darker ice or debris. This, in turn, leads to more solar radiation absorption, further increasing GST, and thereby creating a positive feedback loop that exacerbates glacier melting.

Considering that there are different methods for calculating albedo and that it is done in different ways for different sensors (Liang 2001), we used the following relationship

to calculate albedo (Smith 2010). This approach has been used frequently for albedo calculation across different land covers (Alves et al. 2017; Bastiaanssen et al. 1998; Han et al. 2016; Ren et al. 2023).

$$\alpha = \sum (\omega_{\lambda} \times \rho_{\lambda}) \tag{1}$$

In Eq. 1, ω_{λ} is the weight coefficient for each band, ρ_{λ} is the reflectance value in different bands, and α is the surface albedo.

For the purpose of investigating the association between GST and glacier albedo, comparable Landsat 5, 7, and 8 imageries as employed for GST assessment were used.

3.3 Snow Cover and Debris-Free Area Delineation Using Landsat Optical Images

Within the context of this research, a computation of the extent of both debris-free (including all snow cover, clean ice, and firn regions) and debris-covered areas was conducted for each available Landsat satellite image used for GST analysis. This was undertaken for two primary purposes. First, it aimed to assess the efficacy of deriving the overall GST from the domain occupied by debris-free regions. The rationale behind this lies in the impact of debris on the glacier’s surface albedo, which diminishes its reflective properties, leading to heightened solar radiation absorption and subsequent temperature elevation. Conversely, regions devoid of debris display an elevated albedo, resulting in increased reflection of solar radiation and, consequently, cooler temperatures. Thus, analyzing the fluctuations in the extent of snow cover and debris-free areas can provide valuable insights into one of the most pivotal drivers of GST alterations.

Second, for the purpose of evaluating alterations in GST across the domains of glacier surfaces characterized by the

presence or absence of debris cover, it is imperative to establish precise boundaries outlining the expanse of debris-free regions within each satellite image. It is noteworthy that the area encompassed by debris-free regions, which encompasses snow cover, clean ice, and firn regions, exhibits marked variability over the year. This variability is noticeable even in sequential Landsat images acquired at 16-day intervals. As a consequence, to ensure the precision of GST analysis, it becomes necessary to distinctly demarcate the areas occupied by debris-free and debris-covered regions for each discrete image. This methodological approach embodies a dynamic strategy, affording the initial separation of these two categories, thus facilitating the subsequent computation of GST with heightened precision.

In this study, the Landsat green and short-wave infrared spectral bands were employed to ascertain the extent of debris-free regions within the study area. This determination was achieved through the utilization of the normalized difference snow index (NDSI) methodology, as denoted by Eq. 2, and a threshold value of 0.45 was used for extracting the Alamkouh glacier debris-free boundaries. It is noteworthy that this particular index has found application in various scientific contexts, including the estimation of snow-covered terrain (Zhang et al. 2013; Zhu and Woodcock 2014), glacier inventory assessment (Wu et al. 2015; Zhang and Zhang 2017), glacier retreat analysis (Thapliyal et al. 2023), and the discrimination of debris-free segments from debris-covered regions within glacier expanses (Rastner et al. n.d.). In Eq. 2, $\text{Band}_{\text{Green}}$ and $\text{Band}_{\text{SWIR}}$ are referred to the green and short-wave infrared bands of the satellite images used.

$$NDSI = \frac{(\text{Band}_{\text{Green}} - \text{Band}_{\text{SWIR}})}{(\text{Band}_{\text{Green}} + \text{Band}_{\text{SWIR}})} \quad (2)$$

3.4 Meteorological Data

Meteorological parameters are important drivers of glacier GST change due to their direct influence on glacier energy and mass balance, thereby shaping glacier behavior and responses to climate variability. In this study, an analysis of the influence of key climate variables, including air temperature, precipitation, cloud cover, and snowfall water equivalent, on the increase of GST was done. Understanding these meteorological influences is vital for comprehending glacier dynamics and their responses to changing climates. For this purpose, the Global Land Data Assimilation System (GLDAS) dataset, a valuable resource for understanding climate-related processes and their interactions with glacial environments, was used (Rodell et al. 2004). The GLDAS dataset offers a comprehensive repository of gridded meteorological and hydrological data, incorporating observations from a network of ground-based stations and satellite mea-

surements. For this study, we accessed monthly GLDAS-2 data with a spatial resolution of about 0.25 degree (about 25 km) in both latitude and longitude for air temperature, precipitation, cloud cover, and snowfall water equivalent, spanning a multiyear period from 1985 to 2020, encompassing regions proximate to the target glaciers. Because the spatial resolution of GLDAS data is much lower than the area of selected glacier, no further processing (such as interpolation or elevation correction) was done, and the information from the pixel of the gridded dataset that comprises Alamkouh glacier was extracted directly. In addition, monthly values were processed by averaging (for air temperature and cloud cover fraction data) and aggregation (for precipitation and snowfall water equivalent) to generate annual data and time-series analysis.

3.5 Spatiotemporal Change Analysis Methodology

For the assessment of spatial variations in GST across the Alamkouh glacier, we initiated the analysis by excluding monthly GST maps during the accumulation period, spanning from October until April. This exclusion was essential because, during the accumulation season, the glacier surface remained entirely shrouded by snow, ensuring that GST remained consistently below the 0 °C threshold across the entire glacier surface. In such conditions, estimating the trend of positive or negative changes in GST becomes particularly challenging and is often prone to substantial margins of error. Furthermore, the omission of data from the accumulation season was imperative to facilitate the distinct examination of GST changes in the debris-free and debris-covered areas. Thus, it is crucial to underscore that our spatial change analysis exclusively pertains to the ablation months and cannot be extrapolated to encompass the entire annual cycle.

In the pursuit of assessing the spatial dynamics of GST, this study employed two distinct methodologies:

First, annual GST maps were formulated through the averaging of GST maps over the ablation months. Subsequently, a continuous spatial trend analysis was employed to elucidate the annual GST variations spanning the entirety of the glacier area. Annual GST maps are pivotal for interpreting the patterns of GST alterations across distinct units and regions of the glacier, facilitating an in-depth analysis of the relationship between glacier hypsometry (elevation distribution) and GST changes, as well as an exploration of the correlations between GST changes, ice-thinning rates, and alterations in albedo. The Mann–Kendall trend test (MKTT) and Sen’s slope estimator were applied to show whether there were upward or downward trends in the multitemporal GST datasets across the glacier area, debris-covered and debris-free regions, and glacier flow units. In addition, the present approach was used to determine

any trends in glacier surface albedo, debris-free areas, and meteorological datasets. Since there are chances of outliers interfering as the extreme GST (and other glacial parameters)—especially extremely cold GSTs due to unusual snowfall in warm months—nonparametric MKTT is more appropriate because MKTT is based on the significance of discrepancies and not on the random values (Sulaiman et al. 2015). It should be considered that one of the main requirements of MKTT and Sen’s slope estimator is that there be no autocorrelation. However, neither normal nor linear distribution of data is required (Gocic and Trajkovic 2013). In order to ascertain the spatial trend of each pixel within a multidimensional annual GST and albedo maps, we used the “generate trend raster” tool within the ArcGIS Pro software (Esri; Redlands, CA, USA). Subsequently, we employed the Mann–Kendall test to discern the statistical significance of trends within our annual GST time series. More details about the calculation of MKTT and Sen’s slope estimator have been provided by Gocic and Trajkovic (2013), and here we focus only on the analysis of the results obtained.

Second, the temporal domain under investigation was partitioned into four approximate decadal periods encompassing the years 1985–1990, 1990–2000, 2000–2010, and 2010–2020. Within these delineated periods, mean GST values were calculated specifically over the ablation months. Decadal GST maps were leveraged in select spatial analyses, including the delineation of GST profiles along glacier flow lines, the generation of GST histograms spanning distinct temporal intervals, and an in-depth examination of the relationship between GST values and elevation across these discrete time periods.

Unlike spatial change analysis, in temporal change section, both accumulation and ablation months were included in trend analysis. The procedure for temporal GST change analysis was as follows: a) All available images over both accumulation and ablation seasons were processed, and cloudy pixels were removed from images, b) monthly GST maps were reconstructed by averaging all available images where cloudy pixels were gathered from the other non-cloudy images, c) annual GST maps were created for each year by averaging the monthly maps, and e) using the Mann–Kendall trend analysis, the temporal changes across the different parts of the glacier were analyzed (including the entire glacier surface, over the glacier flow units, and over debris-free and debris-covered areas).

4 Results

4.1 Spatial Variation of GST

Figure 3 presents the ultimate outcome of the annual GST change, as ascertained through the utilization of the Sen’s slope estimator method applied comprehensively across the expanse of the Alankouh glacier. The results obtained illuminate the dynamic nature of the glacier’s surface temperature, revealing spatial fluctuations ranging from a minimum of 0 to a maximum of $+0.2^{\circ}\text{C/a}$ over the period spanning 1985 to 2020 (over the ablation season from May to September). The calculated mean annual GST increment, encompassing the entirety of the glacier area, amounts to 0.086°C/a , signifying an aggregate rise of approximately 3°C over the ablation seasons of the past 36 years. The most substantial GST escalation is observed within the central region of flow unit 1, whereas GST alterations in other sectors of the glacier exhibit less pronounced changes. While a discernible pattern in GST change across the glacier’s surface remains elusive, it is noteworthy that high-altitude regions exhibit a more substantial GST increase in com-

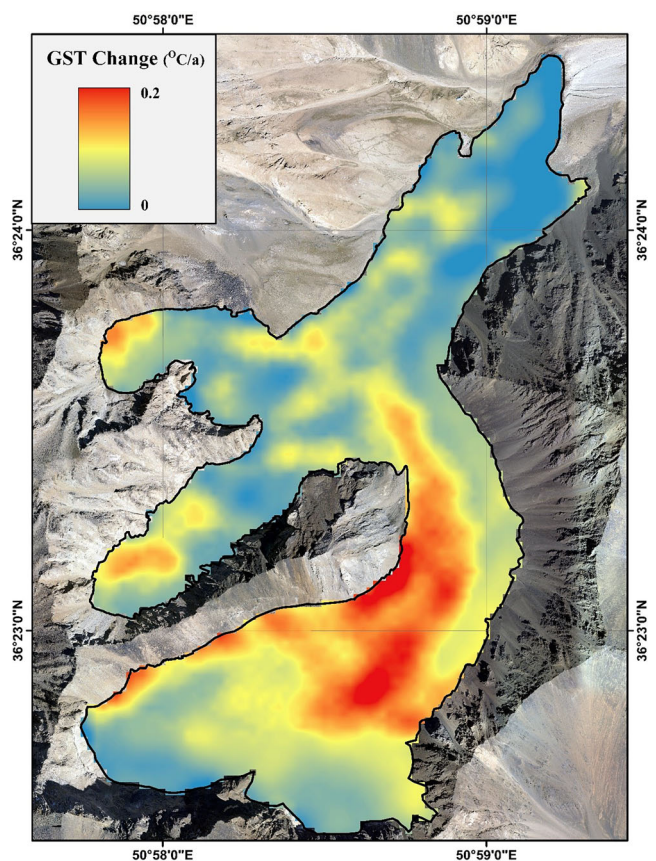


Fig. 3 Spatial distribution of the annual glacier surface temperature change from 1985 to 2020, calculated from the Sen’s slope estimator during the ablation season (from May to September) across the Alankouh glacier

parison to their lower-altitude counterparts. Furthermore, localized GST hot spots are discernible within the elevated areas of flow units 2 and 3; however, their GST increases, in general, are relatively less when compared to flow unit 1.

In our study area, the rate of change in the GST was 1.6 times greater than the rate of change observed in limited areas where GST changes have been studied. For example, a similar approach to the current study was employed to analyze the Hailuoguo glacier, located in the southeastern

region of the Tibetan plateau, using Landsat 5 and 8 satellite imagery (Liao et al. 2020). This study revealed an increase in temperature of 0.054 °C/a between 1990 and 2018.

Figure 4a–d illustrates the spatial patterns of the mean decadal GSTs that occurred during the ablation seasons, along with the corresponding mean glacier GSTs for the whole glacial area throughout the ablation season. The obtained results indicate that from a minimum of 7.2 °C for the period 1985–1990 to a maximum of 11.4 °C for the period

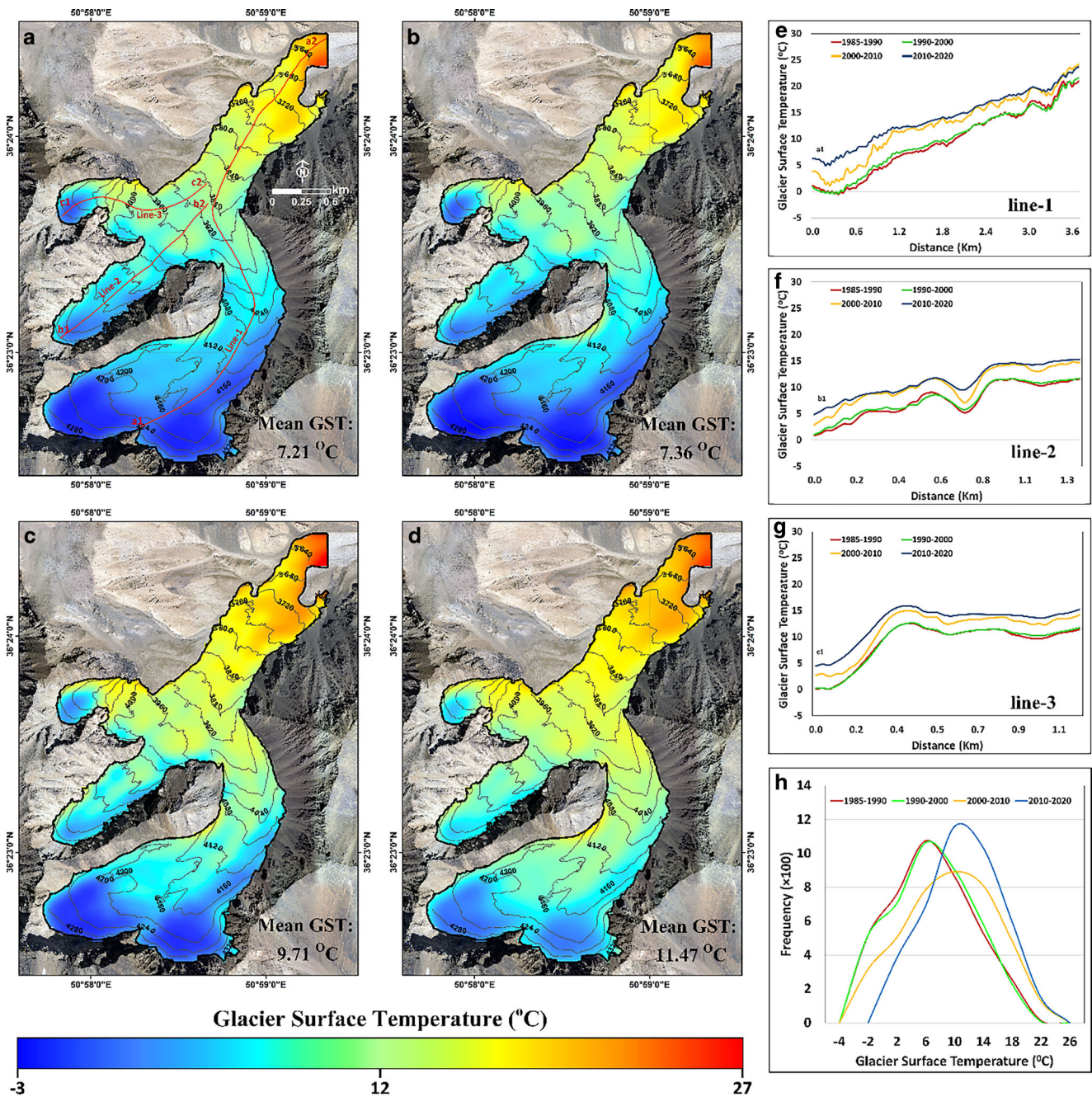


Fig. 4 Spatial distribution of the decadal mean glacier surface temperature (GST) during the ablation season (from May to September) across the Alankouh glacier during the following periods: **a** 1985–1990, **b** 1990–2000, **c** 2000–2010, and **d** 2010–2020. GST along the central flows for **e** line 1, **f** line 2, and **g** line 3. The positions of the lines are depicted in **(a)**. **h** GST histograms for the different periods

2010–2020, the mean GST of the glacier has gradually increased. Since 1985–1990, the mean GST has remained relatively constant; however, from 1990–2000 to 2000–2010, the GST has risen by an estimated 2.3 °C per decade (between 1990–2000 and 2000–2010, the mean GSTs were approximately 7.3 and 9.7 °C, respectively). There has been a continuation of this trend between the 2000–2010 and 2010–2020 periods; however, there has been a decrease in the rate of growth of the GST in comparison to the previous decadal period, reaching about 1.7 °C per decade in the most recent period. Two explanations should be provided to elucidate why the average GST was positive in the mean decadal maps. First of all, only the ablation seasons of the years are included in these maps; second, the majority of the glacier surface is debris covered at this time of year, and only a small part of the glacier surface is exposed ice with a temperature below 0 °C at these months. This means that the mean temperatures expressed do not represent the mean annual surface temperature of the glacier, and it is obvious that the average temperature of the glacier is less than 0 °C on an annual basis.

Figure 4e–h illustrates the GST along the central flow lines between four distinct decadal periods. The figures demonstrate the temporal variation in GST over the course of the decades. In line 1 (across the flow unit 1), the GST was approximately 0 °C at the highest point of the glacier surface in areas devoid of debris, and it increased steadily to more than 20 °C at the terminus of the glacier, where the debris layer is assumed to be thickest. A comparable trend is discernible in lines 2 and 3, in which the GST was observed to be higher in the low-elevation regions of the glacier. A detailed analysis reveals that there is a point of inflection in line 2 and line 3 at a distance of approximately 0.7 km and 0.4 km, respectively. At a distance of 0.4 km from the highest point of line 3, the average GST remained constant and did not vary until the completion of the survey. Because the altitude of the glacier surface along the line extending from 0.4 km to 1.2 km did not demonstrate a significant variation. Additionally, line 2 exhibited a localized decrease in GST at a distance of 0.7 km, followed by a gradual increase in GST up to the end of line 2 at 0.8 km. In all the investigated epochs, the computed GST for the periods 1985–1990 and 1990–2000 were found to be very similar, and in many cases they were identical. This is particularly pertinent in lines 2 and 3, where the glacier surface is completely obscured by debris. In contrast, the greatest variation in GST was observed between the 1990–2000 and 2000–2010 time frames, with a marked transformation in all profiles. Nevertheless, the alteration in the GST between the 2000–2010 and 2010–2020 time frames is once more diminished across all categories.

The GSTs of the 2000–2010 and 2010–2020 periods in lines 2 and 3 are more similar in comparison to line 1. As

previously discussed, this can be attributed to the presence of debris covers in these regions. This is mainly due to the fact that, based on field observations and high-resolution unmanned aerial vehicle (UAV) image reviews, there are no ice cliffs, supraglacial lakes, or debris-free areas that can cause GST heterogeneities in flow units 2 and 3 (Karimi et al. 2021b).

The histogram of the GST over the four decadal periods (Fig. 4h) reveals a marked shift toward higher surface temperatures (approximately 4 °C per decade) in the two most recent decades (2000–2020). The minimum and maximum rate of GST experienced an augmentation over the last decade (2010–2020), with the minimum rate increasing from –2 to +2 °C per decade. These histograms indicate that not only the mean GST experienced a 4 °C increase from the 1985–1990 period to the 2010–2020 period, but the minimum GST also shifted from negative to positive values. The elevated rate of minimal GSTs has been shown to significantly contribute to the accelerated melting of glaciers.

As illustrated in Fig. 5, the fluctuations in the GST with respect to altitude were analyzed across mean decadal GST maps. The results demonstrate a highly significant and negative correlation ($R^2 = -0.8$) between GSTs and elevation, with an elevation gradient of approximately –0.03 °C per 100 m. This anticipated trend is replicated across all epochs with only slight deviations. Nevertheless, there is evidence of slight variations in the GST gradient. The GST gradient exhibited a decrease from –0.029 °C per 100 m during the 1985–1990 and 1990–2000 periods, to –0.031 °C per 100 m between 2000–2010, before reverting to –0.026 °C per 100 m in the most recent decade (2010–2020). Furthermore, the mean GST of the debris-free area and transition zone (the boundary between debris-covered and debris-free regions on the surface of glacier) increased by approximately 3 °C over the past decade, compared to the previous mean of –3 °C. The homogeneity of GST in both debris-free and debris-covered zones from 2010 to 2020 was less than in other periods. This heterogeneity may be associated with an increase of debris cover area across the total glacier surface, as evidenced by debris-free area change results (Sect. 5.2).

As illustrated in Fig. 5, the lowest GST was observed in the region at the summit of the glacier that was free from any accumulation of debris. Conversely, the highest GST was located at the terminus of the glacier. The transition zone and debris-free region of glacier throughout all time periods exhibit a high degree of variability, in contrast to the debris-covered zones, which display a much more homogeneous nature. This incongruity resulted mainly because of the exposure of debris covers, the emergence of ice-melting zones, and the wide variations in the depth of the debris covers at transition zone. It has been observed that similar patterns of variability in the amount of GST in

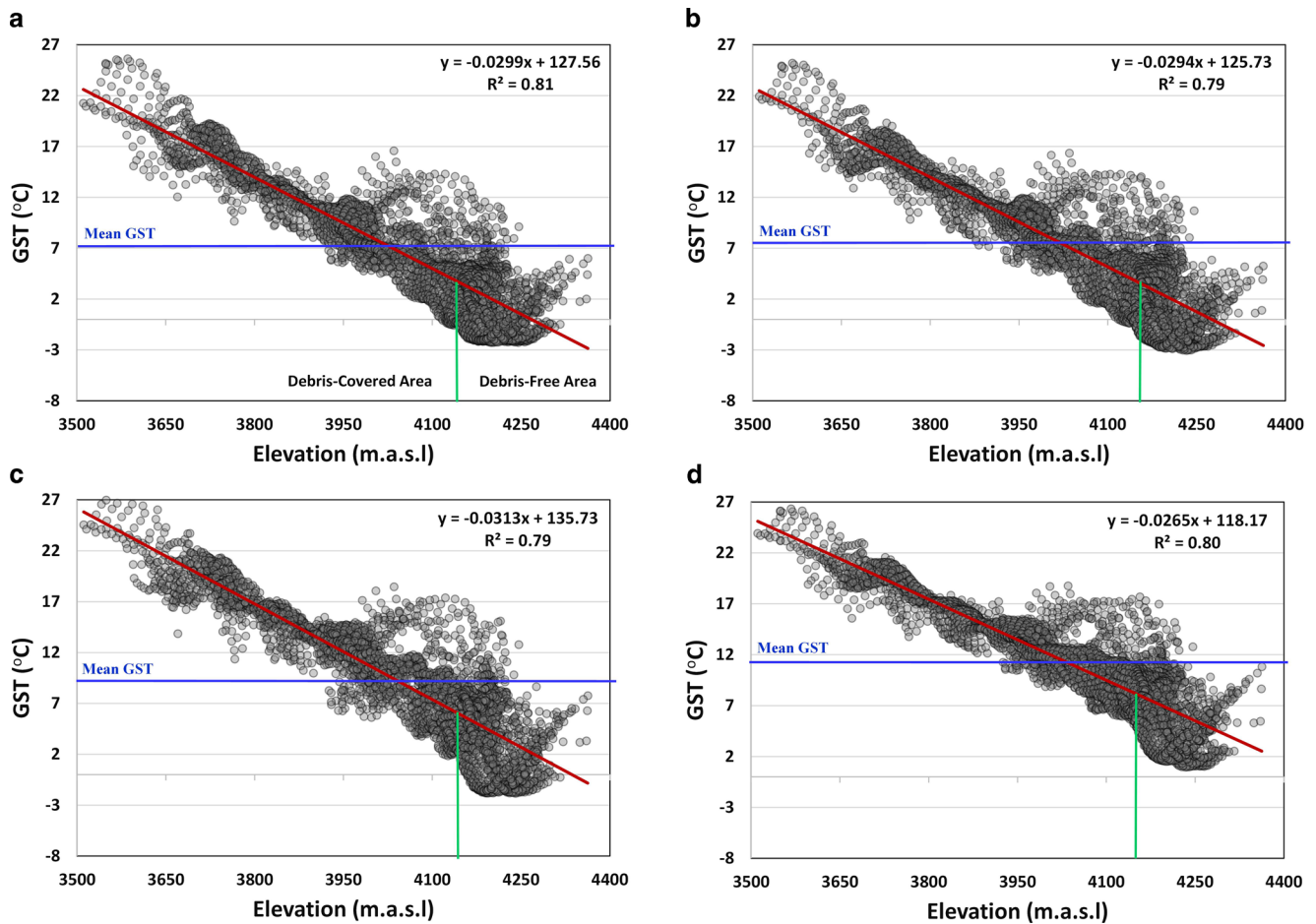


Fig. 5 Variation of glacier surface temperatures (GSTs) with elevation during **a** 1985–1990, **b** 1990–2000, **c** 2000–2010, and **d** 2010–2020. In equations, “y” denotes “GST,” and “x” denotes elevation

debris-free areas of glaciers covered with debris have been documented in other glaciers of the same type (e.g., Tibetan plateau; Liao et al. 2020).

It should be noted that the linear equations in Fig. 5 hold validity solely within the altitudinal spectrum encompassing the glacier’s specific location, spanning from 3500 m to 4400 m, and should not be extrapolated to altitudes either higher or lower.

In Fig. 6a, we have presented a spatial representation of the monthly variations of GST, aiming to elucidate the temporal variation of GST within each individual pixel across the course of a year. This map was calculated based on all the available cloud-free scenes per year and then averaged over the 36 years. The outcomes obtained from this analysis unveil a compelling correlation between monthly GST variations and the topographical factor of elevation. With ascending elevation, particularly toward higher-altitude regions, there is a discernible decline in GST values, transitioning from a maximum of 18 °C at the glacier snout to a minimum of 10 °C at the highest point of the glacier.

Concurrently, it is noteworthy that the map depicting monthly GST variation exhibits a notably robust association with the mean annual GST maps, as presented in Fig. 4a. Consequently, it is observed that the highest GST variation coincide with regions featuring the highest mean annual GST values, while the lowest GST variations align with areas characterized by the lowest mean annual GST values.

This observed relationship between monthly GST variation and mean annual GST is closely linked to the dynamic nature of snow cover throughout the year. In lower-elevation sections of the glacier, substantial variability in snow cover is evident, thereby leading to heightened levels of GST variation throughout the year. Conversely, in regions of elevated altitude, particularly those devoid of debris, the glacier surface is predominantly covered by ice, snow, or firn, resulting in comparatively minimal fluctuations in GST.

4.2 Temporal Variation of GST

Figure 6b is a graphical representation of the average monthly GST over an extended period of time, thereby

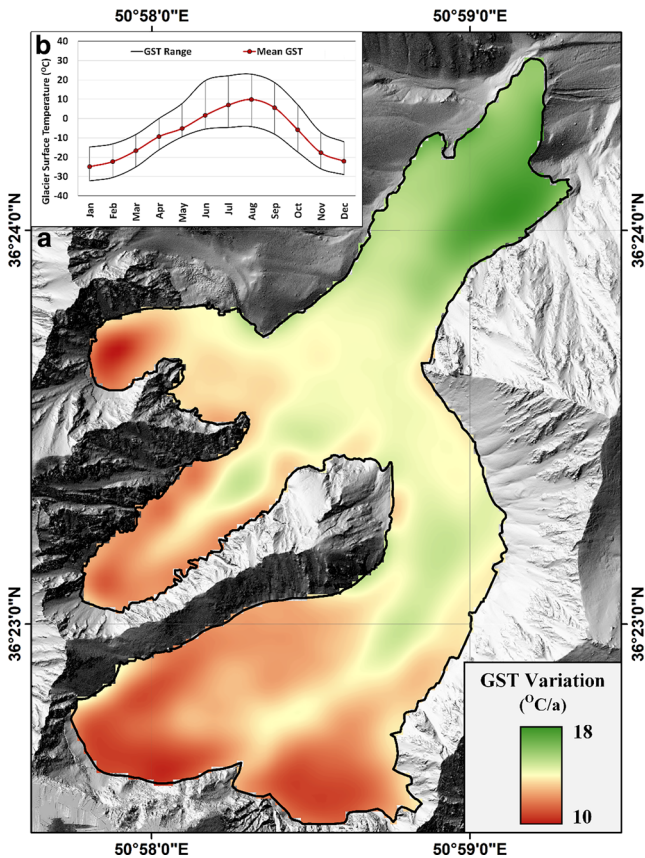


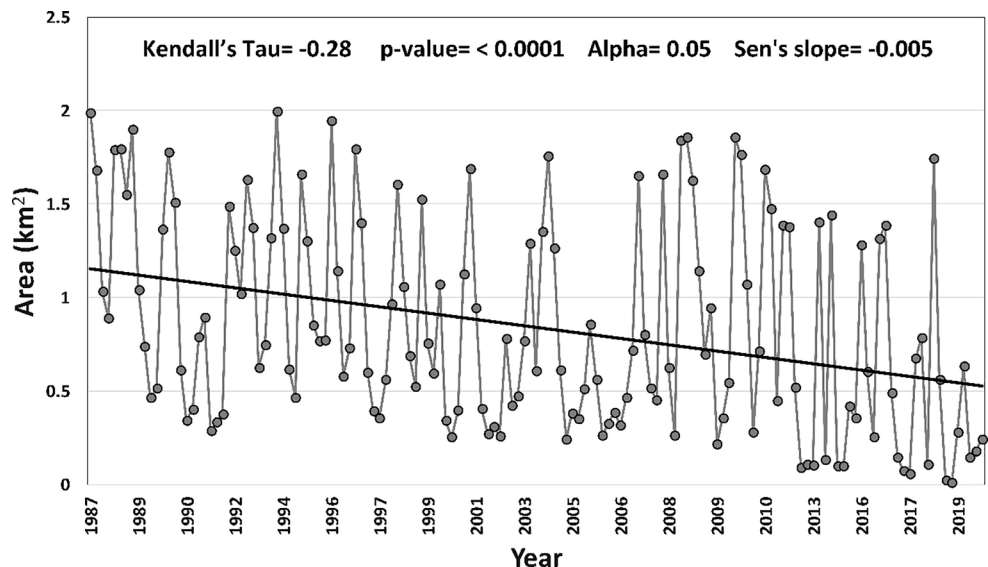
Fig. 6 a Monthly spatial glacier surface temperature (GST) variation (calculated based on all the available cloud-free scenes per year and then averaged over the 36 years). b Monthly minimum, maximum, and mean GST of Alankouh glacier

demonstrating the fluctuation of GST from month to month. The results of the analysis demonstrate that the monthly oscillations of the GST at the glacier surface are substantial, with the minimum temperature of -25°C recorded in January and the maximum temperature of 10°C registered in August.

The most critical factor contributing to the 35°C oscillations is the presence of a debris-covered surface on the Alankouh glacier. The frequent fluctuations in GST in certain glaciers can be attributed to the seasonal alternation between highly frigid ice and snow cover during the months of accumulation and warm debris cover during the ablation season. If the entire glacial surface is devoid of debris or has a covering of debris during the warmer months, the amount of fluctuation in GST would be significantly reduced. Furthermore, the amplitude of the GST fluctuations during the ablation months (May to September) is greater than during the cooler months. The primary factor driving this phenomenon is the presence of a uniform snow cover over the glacier surface during the accumulation season, in contrast to the more heterogeneous landscape of glacier features (including debris-covered areas, debris-free areas, supraglacial ponds, ice cliffs, etc.) observed during the ablation months, each of which has its own distinct thermal characteristics. On the other hand, the GSTs demonstrate a lower degree of variability during the accumulation season, when snow accumulates gradually beginning in November and persists on the glacier surface until midsummer.

Figure 7 illustrates the area of glacier surface below the 0°C isotherm for the ablation season, from May to September. Indubitably, with the glacier surface area being entirely masked by snow during the accumulation season, the portion of the glacier’s surface below the 0°C isotherm boundary remains constant, resulting in the inability to obtain

Fig. 7 Variation of glacier surface area below the 0°C isotherm line in ablation season (from May to September) from 1985 to 2020



meaningful results. As a result, this analysis was exclusively conducted during the ablation season. The results obtained demonstrate that the area of the glacier surface below 0°C isotherm has shown a particularly pronounced decline at a rate of $-0.005\text{ km}^2/\text{month}$ and a total decline of about 0.77 km^2 during the ablation season from 1985 to 2020. The results of the analysis of the area of the glacier surface below 0°C temperature suggest that the proportion of the debris-free area of the Alankouh glacier has decreased since 1985, while the extent of the debris-covered area has increased. This issue is verified in Sect. 5.2.

In the continuation of temporal analysis, the long-term annual GST change from 1985 to 2020 was investigated across the entire glacier surface area, over glacier flow units, and over the debris-covered and debris-free surfaces. In this section, mean GST was calculated during both the accumulation and ablation seasons. The results of this analysis are presented in Fig. 8. The Mann–Kendall test and Sen's slope estimators were employed to determine whether there were significant ascending or descending trends present in the temporal GST datasets. The analysis of the data yielded results that demonstrate a statistically significant and meaningful trend in GST across the entire glacier surface area,

Fig. 8 Long-term annual glacier surface temperature change from 1985 to 2020 (a) over an entire glacier surface area, (b) over three different flow units of the glacier, and (c) over debris-free and debris-covered glacier areas

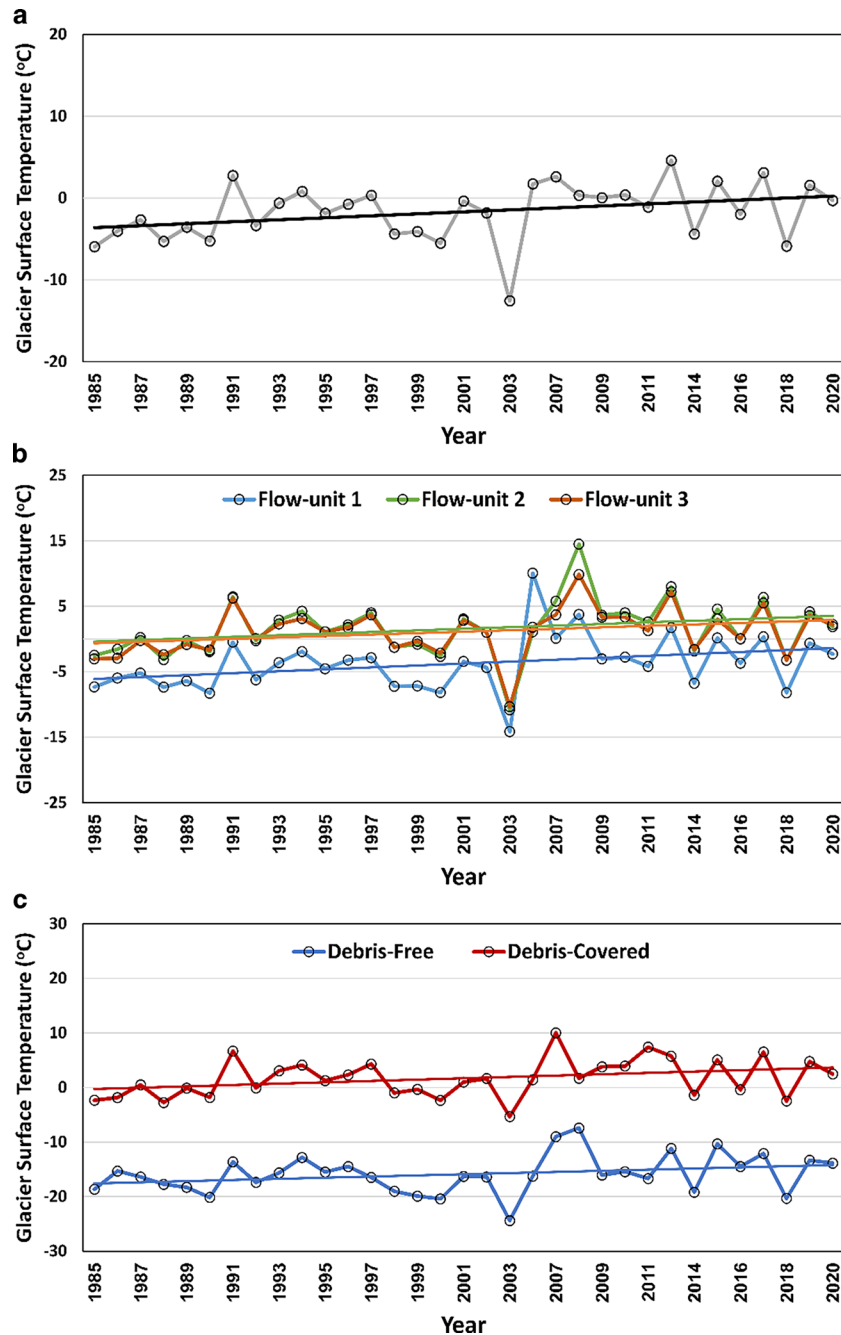


Table 1 Results of statistical tests for annual glacier surface temperature (GST) change over the period 1985–2020

GST	<i>p</i> -value	Minimum (°C)	Maximum (°C)	Mean (°C)	Standard deviation (°C)	Kendall’s tau	Sen’s slope
Whole glacier area	0.031	−12.5	4.6	−1.6	3.5	0.26	0.133
Debris-covered area	0.034	−5.3	10.03	1.68	3.4	0.26	0.139
Debris-free area	0.125	−24.4	−7.4	−15.8	3.5	0.19	0.097
Flow unit 1	0.027	−14.1	10.04	−3.7	4.3	0.27	0.150
Flow unit 2	0.061	−10.8	14.4	1.5	4.3	0.23	0.123
Flow unit 3	0.027	−10.3	9.8	1.1	3.7	0.27	0.123

as well as over the debris-covered and debris-free areas and all flow units, at a confidence level of 95% (Table 1). It is worth noting that the *p*-values less than the significance level (0.05) must be considered as a remarkable trend in the Mann–Kendall time series analysis. The *p*-values for all parts of the glacier were found to be significantly less than 0.05, thus indicating a pronounced trend in GST.

The results of the annual GST of Sen’s slope estimator are shown in Table 1. The obtained results indicated that the greatest warming trends over the past 36 years were observed in the GST over debris-covered areas (0.139°C/a) and flow unit 1 (0.150°C/a). Furthermore, a quantitative evaluation of the GST time series indicated a substantial rise in surface temperature in debris-free areas (0.097°C/a), flow unit 2 (0.123°C/a), and flow unit 3 (0.123°C/a). The overall magnitude of the glacier area’s temperature has been increasing at a rate of 0.133°C/a since 1985, which is indicative of a 4.7°C rise in the last 36 years during both accumulation and ablation seasons. It is noteworthy that, after a spatial change analysis was conducted (which excluded the accumulation season over glacier surface from the analysis), the magnitude trend of the entire glacier area was approximately 0.086°C/a, resulting in a total increase of 3°C. These results indicate a higher warming rate during the ablation season compared to the rest of the year.

5 Discussion

5.1 Glacier Hypsometry and GST Change

For the purpose of analyzing spatial change, we investigated the disparities in long-term spatial GST change (changes between the 1985–1990 and 2010–2020 periods) in relation to the topographical characteristics (hypsometry) of glaciers. In Fig. 9, the long-term spatial change in GST has been averaged across 10-m elevation intervals and then graphed against the corresponding elevation. These results illustrate that considerable variations in the GST are evident in the higher-altitude regions of the whole glacier, whereas the GST experienced less fluctuation in the lower-elevation area. It is evident that with progression toward higher altitudes, the rate of increase in GST increases cor-

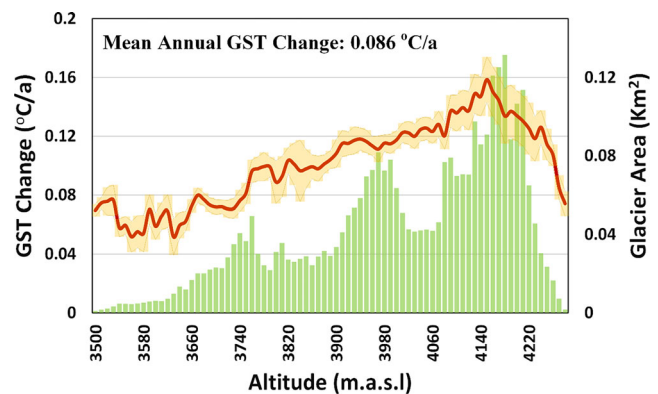


Fig. 9 Relationship between glacier hypsometry and glacier surface temperature (GST) change curve over the ablation season for the whole glacier area. *Yellow shaded* area shows the standard deviation of GST change over each elevation bin

respondingly, and conversely, with movement toward lower altitudes, the rate of GST increase diminishes. Nevertheless, beyond the transition zone of the glacier, this regulation was suddenly disrupted. This result reveals that the rate of increase in GST is comparatively less in the debris-free region (altitudes greater than 4100m above sea level) as compared to the lower altitudes. It has been observed that in areas where the ice is pristine, the rate of increase in GST diminishes with an increase in elevation.

5.2 Relationship Between GST Change, Debris-Free Area Change, and Glacier Albedo Change

Within this section, an examination was undertaken to analyze the ratio of debris-free terrain, calculated via the NDSI, with the objective of highlighting the detectable changes spanning the temporal spectrum from 1985 to 2020 across the entirety of the glacier’s surface. A comparative analysis was executed, comparing the extent of debris-free area vis-à-vis the total glacier surface area during both the accumulation and ablation seasons, thereby yielding the calculated ratio of debris-free area. The outcomes derived from this analysis manifest an explicit and statistically meaningful diminishing trend in the proportion of debris-free cover during the investigated time frame, as depicted in Fig. 10a. Specifically, the magnitude of glacier debris-free terrain has

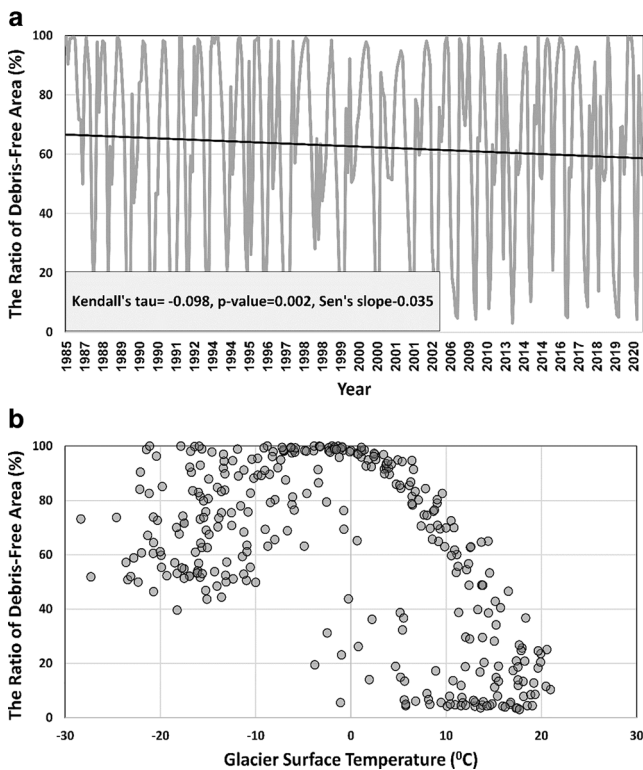


Fig. 10 **a** Monthly ratio of debris-free area over an entire glacier surface area from 1985 to 2020. **b** Relationship between mean glacier surface temperature and ratio of debris-free area

exhibited a compelling and negative monthly rate of change amounting to $-0.035\%/month$ since 1985. This rate translates to a substantial decrease of 15.12% over the course of the past 36 years, encompassing both accumulation and ablation seasons.

Reducing the extent of debris-free regions may constitute a paramount contributing factor in elevating the GST. To assess this potential correlation, we analyzed the mean monthly GST against the mean ratio of glacier debris-free areas, as illustrated in Fig. 10b. The results obtained from this analysis reveal a robust and inverse relationship between the surface temperature of the glacier and the extent of debris-free terrain, specifically within the temperature range from 0°C upward ($R^2=0.55$). Within this range, as the ratio of debris-free areas diminishes, there is a corresponding gradual increase in the surface temperature of the glacier. However, it is noteworthy that this pronounced relationship becomes less discernible when surface temperatures fall below 0°C . In instances when surface temperatures plunge below 0°C , different ratios of debris-free coverage, ranging from 40% to 100% , give rise to significantly divergent surface temperatures on the glacier, spanning from 0°C to as low as -30°C . For instance, even with a 60% debris-free coverage, the surface temperature may plummet to approximately -20°C . In essence, these findings underscore that during the ablation months of the year,

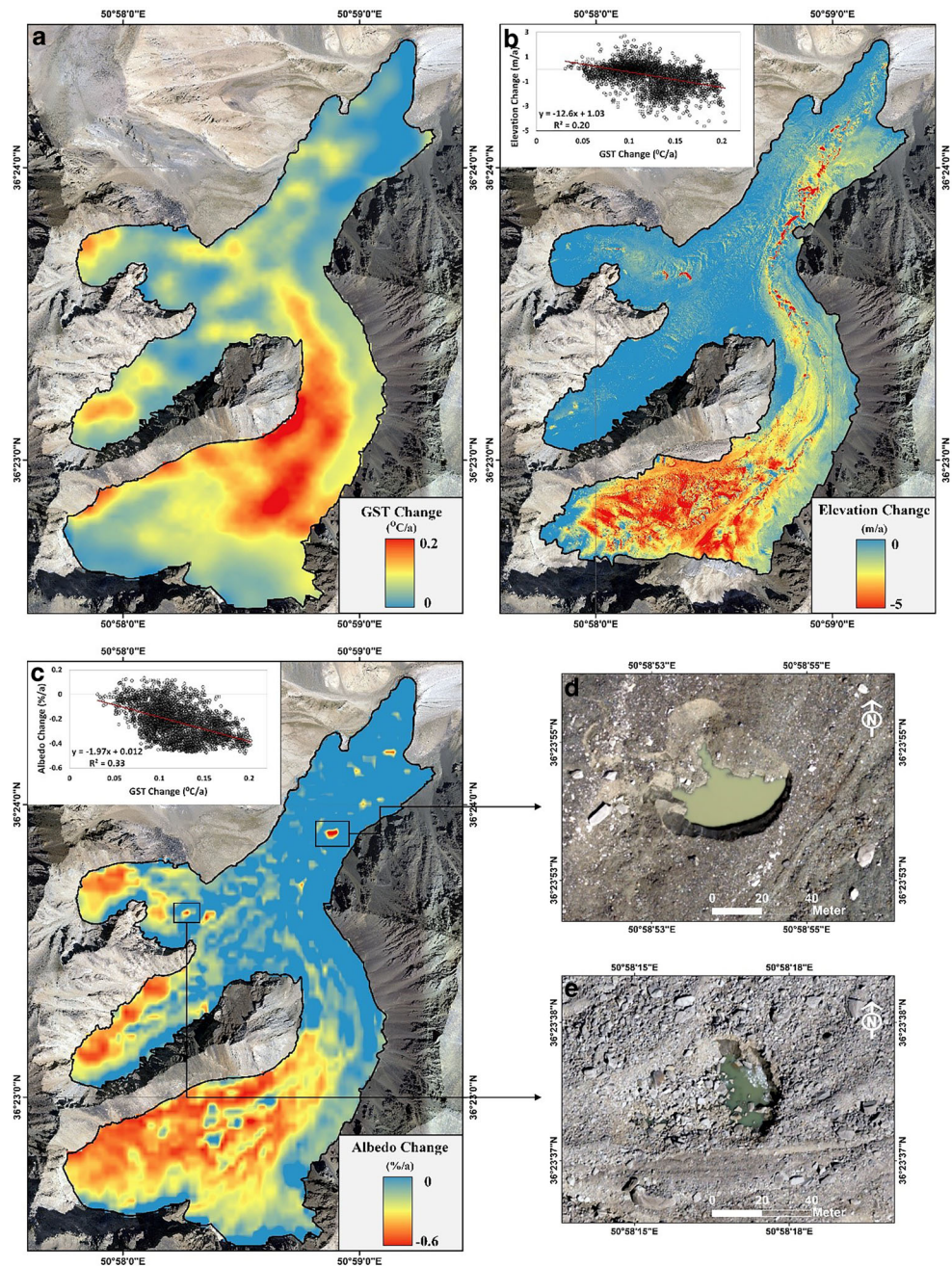
when surface temperatures on the glacier exceed 0°C , the preeminent determinant of surface temperature is the extent of debris-free terrain. However, during the colder months when surface temperatures plunge significantly below 0°C , other variables, such as the entry of extremely cold masses, assume a more decisive and dominant role in shaping surface temperature than the extent of debris-free terrain.

To investigate the correlation between alterations in glacier albedo and changes in GST, we have presented the outcomes of an analysis pertaining to albedo change in Fig. 11c, in conjunction with the results of GST change and elevation change assessments. The analysis of albedo change has yielded insightful findings. Over areas characterized by low elevations, albedo has remained relatively stable and exhibited minimal change throughout the past 36 years. Conversely, considerable alterations in albedo have been observed across high-elevation areas, particularly those designated as debris-free regions and transition zone areas. Within the high-elevation regions, specifically encompassing flow units 2 and 3, the transformations in albedo are notably conspicuous and exhibit a noteworthy correlation with the results of GST change analysis. Remarkably, in these specific regions, as opposed to the elevation change map where no significant elevation variations have been recorded within flow units 2 and 3, a substantial decrease in albedo has occurred. Consequently, this decline in albedo has had the consequential effect of elevating GST within these regions. The findings obtained from this study serve to underscore a discernible relationship between the diminishing extent of snow cover, an evident consequence of the evolving climate patterns, and the intricate dynamics of the surface energy balance within the domain of debris-covered glaciers. The impact of this reduced snow cover, notably observed within the context of the albedo effect, is distinctly substantial. It is intriguing to observe that this impact is less prominent when we extend our examination to the realm of debris-free glaciers.

The most pronounced reduction in albedo was observed in regions characterized by the presence of glacier ponds and ice cliffs. This phenomenon, as illustrated in Fig. 11d and e, was attributed to the development of these features on the glacier's surface, leading to a substantial decrease in albedo. Consequently, the diminished albedo resulted in heightened solar radiation absorption, subsequently triggering significant alterations in elevation. The examination of alterations in albedo unveils a considerable annual decrease of approximately -0.08 per year across the entirety of the glacier terrain, with the most significant reduction in albedo occurring within flow unit 1. The R^2 quantifying the spatial correspondence between changes in GST and albedo has been ascertained to approximate -0.33 .

In contrast to the GST alterations, the albedo change map exhibits a stronger association with the map depicting ice-

Fig. 11 **a** Glacier surface temperature (GST) change map from 1985 to 2020. **b** Glacier elevation change map from 2018 to 2020 using unmanned aerial vehicle data (Karimi et al. 2021b) and GST change plotted against the elevation change output. **c** Annual albedo change map from 1985 to 2020 and GST change plotted against the albedo change output. **d, e** Development of glacier ponds and ice cliffs over the glacier surface and their corresponding albedo change



thinning rates (Fig. 11a). Notably, areas characterized by higher rates of ice thinning demonstrate a marked decline in albedo. This phenomenon is particularly pronounced in elevated regions, with the most substantial correlation observed in these high-altitude areas.

In order to assess the correlation between the changes in glacier ice-thinning rate and increases in GST, the findings of an annual glacier elevation change analysis conducted using unmanned aerial vehicle (UAV) photogrammetry techniques over the period 2018–2020, as reported by Karimi et al. (2021b), are presented in Fig. 11 alongside the results of the GST change analysis. This study high-

lights discernible disparities in elevation alterations among distinct zones of the glacier, encompassing the debris-free zone at the upper region, areas with a thin debris covering, and the heavily debris-laden downslope where the rate of elevation change in the glacier is notably more pronounced in areas devoid of debris compared to those with substantial debris coverage. Such elevation change patterns are prevalent in heavily debris-covered glaciers and are observable across various regions (Capt et al. 2016).

Although the duration of the study period for examining alterations in elevation is comparatively brief in relation to the period of analysis for GST change, it has been observed

that there has been no alteration in the spatial distribution of elevation changes in the Alamkouh glacier since 2010 (Karimi et al. 2021a), and similar spatial thinning rate have been observed over the study area since the last decade.

The analysis of changes in elevation (as depicted in Fig. 11b) reveals a substantial rate of thinning in flow unit 1, approximately -0.37m/a . Conversely, the rates of elevation changes within flow unit 2 and flow unit 3 were found to be negligible, measuring approximately -0.008m/a and -0.01m/a , respectively. A comparable pattern was observed generally in the alteration of GST, wherein the highest augmentation in GST was observed in flow unit 1, while the least significant alterations were observed in flow units 2 and 3. However, a comprehensive examination revealed that a robust association between these two factors could not be ascertained. In areas characterized by significant augmentation in GST, such as the elevated areas encompassing flow unit 3, the decrease in ice thickness was negligible, and no perceptible modification in ice thickness was detected. Within the flow units 2 and 3, there has been an approximate $0.123\text{ }^\circ\text{C/a}$ rise in the GST, without any alteration in the ice thickness. The absence of robust coherence is likewise apparent in the statistical information. The R^2 for the spatial relationship between changes in GST and changes in

glacier elevation has been determined to be approximately -0.20 . This finding indicates that although it was anticipated that there would be a negative correlation, the results do not demonstrate a statistically significant and substantial relationship between GST and the outcomes of glacier elevation change. Thus, it seems that the increase of GST over the flow units 2 and 3 was not correlated with the glacier surface elevation change, whereas other parameters (e.g., increase in air temperature) are more dominant. Nevertheless, in areas where thick debris covers are not dominant (flow unit 1), the GST increased more significantly as the ice thickness decreased. Because the decrease in ice thickness is accompanied by an increase in debris cover, this leads to a significant increase in GST.

5.3 Meteorological Analysis

This study investigated the temporal dynamics of key climate variables on GST, including air temperature, precipitation, cloud cover fraction, and snowfall water equivalent, using the GLDAS dataset and rigorous statistical analysis techniques. The Mann–Kendall trend test was applied to monthly data series, yielding valuable insights into long-term trends. The results of the analysis, including Kendall's

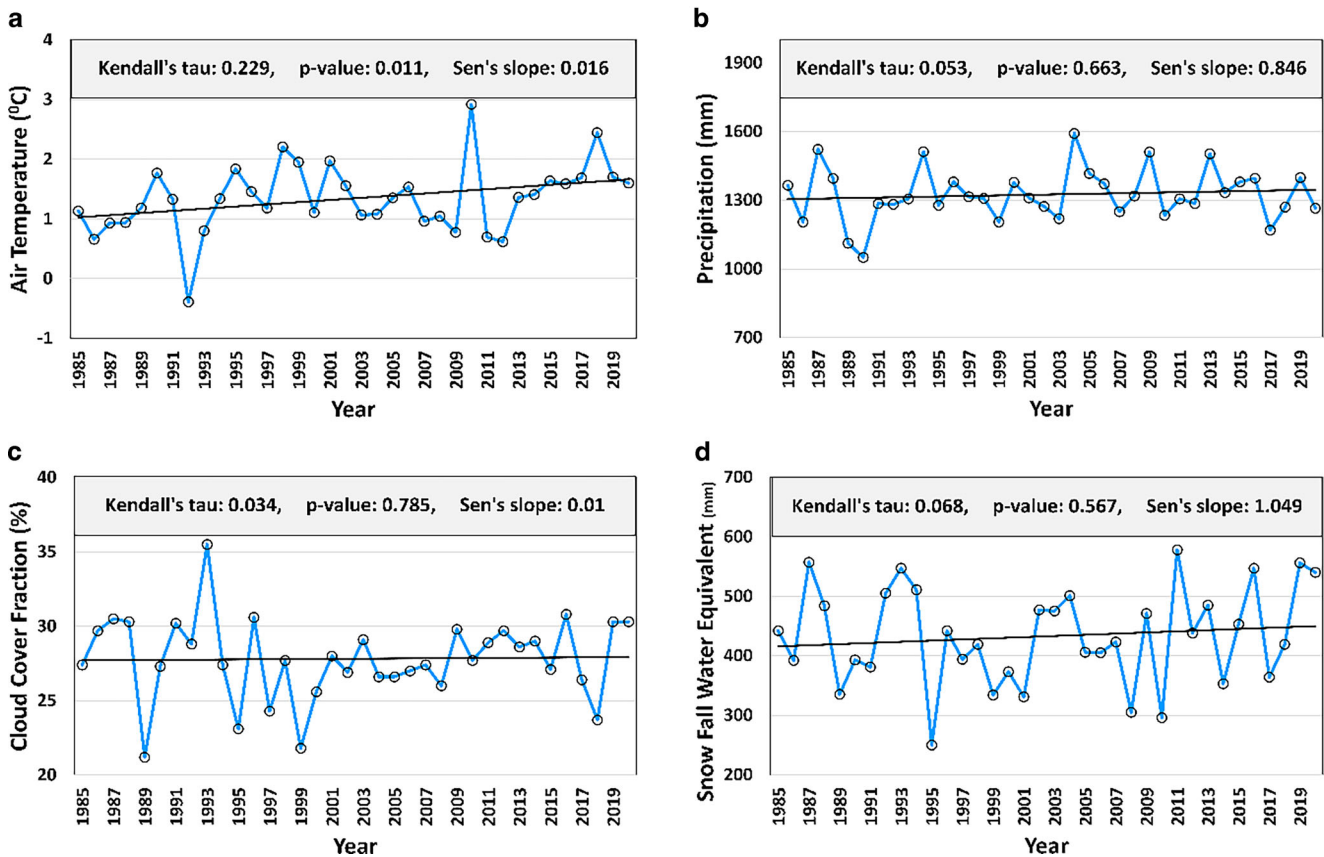


Fig. 12 Long-term annual change in (a) air temperature, (b) precipitation, (c) cloud cover fraction, and (d) snowfall water equivalent over Alamkouh glacier from 1985 to 2020

tau, p -values, and Sen's slope, provide a comprehensive understanding of the observed changes in these climate parameters (Fig. 12).

Our analysis reveals a statistically significant positive trend in annual air temperature (Fig. 12a), as indicated by Kendall's tau (0.229), a low p -value (0.011), and Sen's slope (0.016). This finding implies a gradual increase in air temperature over the observation period, with high potential consequences on GST. It is worth noting that this moderate increase in air temperature over the last 36 years can explain only a small fraction of the pronounced increase in GST. The focus should thus shift to exploring the intricate feedback mechanisms associated with this moderate air temperature escalation, which likely play a far more consequential role in the observed GST increase.

Annual precipitation data (Fig. 12b) display a Kendall's tau value of 0.053, a nonsignificant p -value (0.663), and Sen's slope of 0.846, suggesting a relatively stable trend with minor fluctuations. While precipitation remains relatively consistent, its interactions with temperature may play a crucial role in glacier surface processes.

Cloud cover fraction data (Fig. 12c) exhibit a Kendall's tau of 0.034, a nonsignificant p -value (0.785), and Sen's slope of 0.01. These results suggest minimal trends in cloud cover fraction, emphasizing the inherent variability in cloud dynamics and their limited direct influence on GST.

Analysis of annual snowfall water equivalent data (Fig. 12d) yields a Kendall's tau of 0.068, a nonsignificant p -value (0.567), and Sen's slope of 1.049. These findings imply a modest upward trend in snowfall water equivalent, though not statistically significant.

The observed positive trend in air temperature holds notable implications for glacier surface conditions. Increasing air temperature (about $+0.5^{\circ}\text{C}$ during the last 36 years) can lead to enhanced glacier melt rates and alterations in snowfall patterns. Precipitation, while relatively stable, can indirectly influence GST through interactions with air temperature and albedo. Cloud cover fraction, remaining stable, may not exert a direct influence on GST but can modulate incoming solar radiation. Snowfall water equivalent trends, albeit minor, hint at potential impacts on glacial mass balance during specific seasons.

6 Conclusions

In this study, we conducted an extensive examination of temporal changes in GST for the debris-covered Alamkouh glacier, situated in Iran, spanning the period from 1985 to 2020 and employing multitemporal Landsat 5, 7, and 8 surface temperature products at a spatial resolution of 30 m. Our research was driven by three primary objectives. First, we performed a comprehensive spatiotemporal analysis of

GST gradients, shedding light on the evolving dynamics of this crucial glaciological parameter. Second, we delved into the intricate correlations between GST and a spectrum of glacier variables, including ice thickness changes and albedo. Third, our investigation extended to identifying factors exerting influence on GST, encompassing variables such as air temperature, cloud cover, precipitation, and snowfall, and we harnessed the wealth of data within the GLDAS dataset. These analyses provide insights into the impact of snow-covered related albedo changes and climatic changes on the GST of an extensively debris-covered glacier.

The analytical backbone of this research hinged on robust statistical tools, namely the Mann–Kendall trend test and Sen's slope estimator, which unveiled statistically significant positive or negative trends across the multitemporal parameters we assessed. The overarching pattern in GST changes across the glacier area revealed fluctuations spanning from 0 to $+0.2^{\circ}\text{C/a}$ during the 36-year study period. Notably, the mean annual GST increase for the entirety of the glacier surfaced at 0.086°C/a , signaling a cumulative rise of 3°C over the course of 36 years. Intriguingly, high-altitude regions exhibited more substantial increments in GST compared to their lower-altitude counterparts, although a distinct pattern remained elusive, reflecting the complexity of underlying processes.

The derived decadal GST spatial patterns for the surface of the Alamkouh glacier indicate a decrease in temperature with an elevation. This phenomenon is suggestive of a negative lapse rate, which is a decline in surface temperature with increasing altitude. The gradient of the GST has remained relatively consistent over the past 36 years, with no discernible fluctuations being recorded. The lowest rate of GST was observed in debris-free areas, and it reached its highest level in debris-covered areas. The GST variation was significantly pronounced in areas where debris cover was present due to the presence of debris-covered surfaces, debris-free surfaces, supraglacial ponds, or exposed ice-cliffs. Also, GST values within the transition zone of the glacier exhibit substantial heterogeneity.

Based on the spatial trend analysis, the mean annual GST increment, encompassing the entirety of the glacier area, amounts to 0.086°C/a , signifying an aggregate rise of approximately 3°C over the ablation season of the past 36 years. While based on the temporal trend analysis over both accumulation and ablation seasons, the magnitude of the GST increase was determined to be approximately 0.133°C/a , which equates to a 4.7°C rise in GST over the course of 36 years, indicating a higher warming rate during the ablation season compared to the rest of the year.

Employing the NDSI, we successfully delineated debris-free areas and probed their potential role in GST variations. Our findings unveiled a robust inverse relationship between

GST and the extent of debris-free terrain, further reinforced by the significant reduction in debris-free terrain at a rate of -0.035% per month since 1985, culminating in a substantial 15.12% decline over 36 years, encapsulating both accumulation and ablation periods. The findings of this investigation suggest that the Alankouh glacier has experienced a rise in temperature and a decrease in the debris-free area as a result of global warming and the concomitant increase in air temperature globally.

The outcomes of our albedo analysis unveiled a robust negative correlation between albedo and mean GST, marked by an R^2 of 0.57. This analysis further elucidated a pronounced annual decrease in albedo, approximately -0.08 per year, spanning the entire glacier terrain. Conversely, albedo in low-elevation areas remained remarkably stable over the 36-year period, with conspicuous variations occurring in high-elevation debris-free regions. Nevertheless, our comprehensive examination failed to establish a robust association between the glacier ice-thinning rate and GST change.

This comprehensive analysis highlights the complexity of annual climate trends and their implications for glacier surface conditions. While air temperature exhibits a significant warming trend, other variables remain relatively stable. Understanding the multifaceted influences on glacier surface temperature is crucial for predicting and adapting to ongoing climate changes in glacial environments. Further research is necessary to unravel the intricate interactions among these climate parameters and their cumulative impacts on glacier dynamics.

Acknowledgements This research was financially supported by the Water Research Institute of Iran. Thermal imagery data were gathered from the United States Geological Survey, to which we are grateful for providing us with the data.

Author Contribution **Neamat Karimi:** study conceptualization, methodology, and writing of original draft. **Omid Torabi:** software and data curation, formal analysis. **Amirhossein Sarbazvatan:** writing—review and editing. **Sara Sheshangosht:** software and data curation.

Availability of Data and Materials The datasets generated or analyzed during the current study are available from the corresponding author on reasonable request.

Conflict of interest N. Karimi, O. Torabi, A. Sarbazvatan and S. Sheshangosht declare that they have no competing interests.

References

- Alif H, Vuillaume JF, Johnson BA, Hirabayashi Y (2020) Machine-learning classification of debris-covered glaciers using a combination of Sentinel-1/2 (SAR/optical), Landsat 8 (thermal) and digital elevation data. *Geomorphology* 369:107365. <https://doi.org/10.1016/J.GEOMORPH.2020.107365>
- Alves LER, De Freitas IGF, Gomes HB, Silva FDDS, dos Santos MN (2017) Using Landsat-8 images in the estimation of the surface radiation balance. *J Hyperspectral Remote Sens* 7:91. <https://doi.org/10.29150/jhrs.v7.2.p91-100>
- Anul Haq M, Jain K, Menon KPR (2012) Surface temperature estimation of Gangotri glacier using thermal remote sensing. *Int Arch Photogramm Remote Sens Spat Inf Sci XXXIX-B8:115–119*. <https://doi.org/10.5194/isprsarchives-xxxix-b8-115-2012>
- Azam MF, Srivastava S (2020) Mass balance and runoff modelling of partially debris-covered Dokriani Glacier in monsoon-dominated Himalaya using ERA5 data since 1979. *J Hydrol* 590:125432. <https://doi.org/10.1016/J.JHYDROL.2020.125432>
- Bastiaanssen WGM, Menenti M, Feddes RA, Holtslag AAM (1998) A remote sensing surface energy balance algorithm for land (SEBAL). 1. Formulation. *J Hydrol* 212:198–212
- Bhardwaj A, Joshi PK, Snehamani, Singh MK, Sam L, Gupta RD (2014) Mapping debris-covered glaciers and identifying factors affecting the accuracy. *Cold Reg Sci Technol* 106–107:161–174. <https://doi.org/10.1016/J.COLDREGIONS.2014.07.006>
- Brun F, Berthier E, Wagnon P, Kääb A, Treichler D (2017) A spatially resolved estimate of High Mountain Asia glacier mass balances from 2000 to 2016. *Nat Geosci* 10:668–673. <https://doi.org/10.1038/ngeo2999>
- Cao B, Guan W, Li K, Pan B, Sun X (2021) High-resolution monitoring of glacier mass balance and dynamics with unmanned aerial vehicles on the ningchan no. 1 glacier in the qilian mountains, China. *Remote Sens*. <https://doi.org/10.3390/rs13142735>
- Capt M, Bosson JB, Fischer M, Micheletti N, Lambiel C (2016) Decadal evolution of a very small heavily debris-covered Glacier in an Alpine permafrost environment. *J Glaciol* 62:535–551. <https://doi.org/10.1017/jog.2016.56>
- Chudley TR, Miles ES, Willis IC (2017) Glacier characteristics and retreat between 1991 and 2014 in the Ladakh range, Jammu and Kashmir. *Remote Sens Lett* 8:518–527. <https://doi.org/10.1080/2150704X.2017.1295480>
- Cook M, Schott JR, Mandel J, Raqueno N (2014) Development of an operational calibration methodology for the Landsat thermal data archive and initial testing of the atmospheric compensation component of a land surface temperature (LST) product from the archive. *Remote Sens* 6:11244–11266. <https://doi.org/10.3390/rs61111244>
- Dehecq A, Gourmelen N, Gardner AS, Brun F, Goldberg D, Nienow PW, Berthier E, Vincent C, Wagnon P, Trouvé E (2019) Twenty-first century glacier slowdown driven by mass loss in High Mountain Asia. *Nat Geosci* 12:22–27. <https://doi.org/10.1038/s41561-018-0271-9>
- Duan SB, Li ZL, Zhao W, Wu P, Huang C, Han XJ, Gao M, Leng P, Shang G (2021) Validation of Landsat land surface temperature product in the conterminous United States using in situ measurements from SURFRAD, ARM, and NDBC sites. *Int J Digit Earth* 14:640–660. <https://doi.org/10.1080/17538947.2020.1862319>
- Ermida SL, Soares P, Mantas V, Göttsche FM, Trigo IF (2020) Google earth engine open-source code for land surface temperature estimation from the landsat series. *Remote Sens* 12:1–21. <https://doi.org/10.3390/RS12091471>
- Farajzadeh M, Karimi N (2014) Evidence for accelerating glacier ice loss in the Takht'e Solaiman Mountains of Iran from 1955 to 2010. *J Mt Sci* 11:215–235. <https://doi.org/10.1007/s11629-013-2714-5>
- Gardelle J, Berthier E, Arnaud Y, Kääb A (2013) Region-wide glacier mass balances over the Pamir-Karakoram-Himalaya during 1999–2011. *Cryosphere* 7:1263–1286. <https://doi.org/10.5194/tc-7-1263-2013>
- Gärtner-Roer I, Nussbaumer SU, Hüsler F, Zemp M (2019) Worldwide assessment of national glacier monitoring and future perspectives.

- Mt Res Dev 39:A1. <https://doi.org/10.1659/MRD-JOURNAL-D-19-00021.1>
- Gocic M, Trajkovic S (2013) Analysis of changes in meteorological variables using Mann-Kendall and Sen's slope estimator statistical tests in Serbia. *Glob Planet Change* 100:172–182. <https://doi.org/10.1016/j.gloplacha.2012.10.014>
- Hall DK, Box JE, Casey KA, Hook SJ, Shuman CA, Steffen K (2008) Remote sensing of environment comparison of satellite-derived and in-situ observations of ice and snow surface temperatures over Greenland. *112:3739–3749*. <https://doi.org/10.1016/j.rse.2008.05.007>
- Han C, Ma Y, Chen X, Su Z (2016) Estimates of land surface heat fluxes of the Mt. Everest region over the Tibetan Plateau utilizing ASTER data. *Atmos Res* 168:180–190. <https://doi.org/10.1016/j.atmosres.2015.09.012>
- Hartl L, Felbauer L, Schwaizer G, Fischer A (2020) Small-scale spatial variability in bare-ice reflectance at Jamtalferner, Austria. *Cryosphere* 14:4063–4081. <https://doi.org/10.5194/tc-14-4063-2020>
- Hauser S, Schmitt A (2021) Glacier retreat in Iceland mapped from space : time series analysis of geodata from 1941 to 2018. *PFG J Photogramm Remote Sens Geoinf Sci* 89:273–291. <https://doi.org/10.1007/s41064-021-00139-y>
- Jiménez-Munoz JC, Sobrino JA (2003) A generalized single-channel method for retrieving land surface temperature from remote sensing data. *J Geophys Res Atmos*. <https://doi.org/10.1029/2003jd003480>
- Kane SN, Mishra A, Dutta AK (2016) Preface: international conference on recent trends in physics (ICRTP 2016). *J Phys Conf Ser*. <https://doi.org/10.1088/1742-6596/755/1/011001>
- Karimi N, Farokhnia A, Karimi L, Eftekhari M, Ghalkhani H (2012a) Combining optical and thermal remote sensing data for mapping debris-covered glaciers (Alamkouh Glaciers, Iran). *Cold Reg Sci Technol* 71:73–83. <https://doi.org/10.1016/j.coldregions.2011.10.004>
- Karimi N, Farokhnia A, Shishangosht S, Elmi M, Eftekhari M, Ghalkhani H (2012b) Elevation changes of Alamkouh glacier in Iran since 1955, based on remote sensing data. *Int J Appl Earth Obs Geoinf* 19:45–58. <https://doi.org/10.1016/j.jag.2012.04.009>
- Karimi N, Farajzadeh M, Moridnejad A, Namdari S (2014) Evidence for mountain glacier changes in semi-arid environments based on remote sensing data. *J Indian Soc Remote Sens* 42:801–815. <https://doi.org/10.1007/s12524-013-0343-7>
- Karimi N, Farokhnia A, Sheshangosht S, Bahreinimotlagh M (2021a) Using UAV and satellite image data for analyzing the elevation change of debris-covered glaciers and its associated driving factors. *Environ Earth Sci* 80:577. <https://doi.org/10.1007/s12665-021-09899-7>
- Karimi N, Sheshangosht S, Roozbahani R (2021b) High-resolution monitoring of debris-covered glacier mass budget and flow velocity using repeated UAV photogrammetry in Iran. *Geomorphology* 389:107855. <https://doi.org/10.1016/j.geomorph.2021.107855>
- Karimi N, Sheshangosht S, Farokhnia A (2022) Determining the spatio-temporal variability of glacier surface velocity using high-resolution satellite images and UAV data: Alamkuh glacier, Iran. *Remote Sens Lett* 13:138–150. <https://doi.org/10.1080/2150704X.2021.2000660>
- Karpilo RD Jr (2009) Glacier monitoring techniques. *Geol Monit*. [https://doi.org/10.1130/2009.monitoring\(06\)](https://doi.org/10.1130/2009.monitoring(06))
- Laraby KG, Schott JR (2018) Remote Sensing of Environment Uncertainty estimation method and Landsat 7 global validation for the Landsat surface temperature product. *Remote Sens Environ* 216:472–481. <https://doi.org/10.1016/j.rse.2018.06.026>
- Liang S (2001) Narrowband to broadband conversions of land surface albedo I: Algorithms. *Remote Sens Environ* 76:213–238. [https://doi.org/10.1016/S0034-4257\(00\)00205-4](https://doi.org/10.1016/S0034-4257(00)00205-4)
- Liao H, Liu Q, Zhong Y, Lu X (2020) Landsat-based estimation of the glacier surface temperature of Hailuoguo glacier, Southeastern Tibetan Plateau, between 1990 and 2018. *Remote Sens*. <https://doi.org/10.3390/rs12132105>
- Lovell AM, Carr JR, Stokes CR (2018) Topographic controls on the surging behaviour of Sabche Glacier, Nepal (1967 to 2017). *Remote Sens Environ* 210:434–443. <https://doi.org/10.1016/j.rse.2018.03.036>
- Malakar NK, Hulley GC, Hook SJ, Laraby K, Cook M, Schott JR (2018) An operational land surface temperature product for landsat thermal data : methodology and validation, pp 1–19
- Moussavi MS, Valadan Zoj MJ, Vaziri F, Sahebi MR, Rezaei Y (2009) A new glacier inventory of Iran. *Ann Glaciol* 50:93–103. <https://doi.org/10.3189/172756410790595886>
- Muhammad S, Tian L (2020) Mass balance and a glacier surge of Guliya ice cap in the western Kunlun Shan between 2005 and 2015. *Remote Sens Environ* 244:111832. <https://doi.org/10.1016/j.rse.2020.111832>
- Pellikka PKE, Rees G (2010) Remote sensing of glaciers : techniques for topographic, spatial, and thematic mapping of glaciers. CRC Press, Boca Raton
- Qin Z, Karnieli A, Berliner P (2001) A mono-window algorithm for retrieving land surface temperature from Landsat TM data and its application to the Israel-Egypt border region. *Int J Remote Sens* 22:3719–3746. <https://doi.org/10.1080/01431160010006971>
- Rastner P, Prinz R, Notarnicola C, Nicholson L, Sailer R, Schwaizer G, Paul F On the automated mapping of snow cover on glaciers and calculation of snow line altitudes from multi-temporal landsat data, pp 1–24
- Ren S, Jia L, Menenti M, Zhang J (2023) Changes in glacier albedo and the driving factors in the Western Nyainqentanglha Mountains from 2001 to 2020. *J Glaciol*. <https://doi.org/10.1017/JOG.2023.45>
- Robson BA, Macdonell S, Ayala Á, Bolch T, Nielsen PR, Vivero S (2021) Glacier and Rock Glacier changes since the 1950s in the La Laguna catchment , Chile. *Cryosphere*: 1–34
- Rodell M, Houser PR, Jambor U, Gottschalck J, Mitchell K, Meng CJ, Arsenault K, Cosgrove B, Radakovich J, Bosilovich M, Entin JK, Walker JP, Lohmann D, Toll D (2004) The global land data assimilation system. *Bull Am Meteorol Soc* 85:381–394. <https://doi.org/10.1175/BAMS-85-3-381>
- Rounce DR, Hock R, Shean DE (2020) Glacier mass change in high mountain Asia through 2100 using the open-source python glacier evolution model (PyGEM). *Front Earth Sci* 7:1–20. <https://doi.org/10.3389/feart.2019.00331>
- Sattari F, Hashim M (2014) A Breif review of land surface temperature retrieval methods from thermal satellite sensors. *Middle East J Sci Res* 22:757–768. <https://doi.org/10.5829/idosi.mejsr.2014.22.05.21934>
- Schaeffer BA, Iames J, Dwyer J, Urquhart E, Salls W, Rover J, Seegers B, Schaeffer BA, Iames J, Dwyer J, Urquhart E, Salls W (2018) An initial validation of Landsat 5 and 7 derived surface water temperature for U . S . lakes , reservoirs , and estuaries. *Int J Remote Sens*. <https://doi.org/10.1080/01431161.2018.1471545>
- Smith RB (2010) The heat budget of the earth's surface deduced from space (R.B. Smith; Version: March, 2010) 2 . Solar Radiation (VIS and SWIR) a . Basic equations. *Terrain*: 1–10
- Sobrino JA, Coll C, Caselles V (1991) Atmospheric correction for land surface temperature using NOAA-11 AVHRR channels 4 and 5. *Remote Sens Environ* 38:19–34. [https://doi.org/10.1016/0034-4257\(91\)90069-I](https://doi.org/10.1016/0034-4257(91)90069-I)
- Sulaiman NH, Kamarudin MKA, Mustafa AD, Amran MA, Azaman F, Abidin IZ, Hairoma N (2015) Analisis corak sungai

- Pahang menggunakan kaedah bukan parametrik: Ujian corak Mann Kendall. *Malays J Anal Sci* 19:1327–1334
- Tarca G, Guglielmin M (2022) Using ground-based thermography to analyse surface temperature distribution and estimate debris thickness on Gran Zebrù glacier (Ortles-Cevedale, Italy). *Cold Reg Sci Technol* 196:103487. <https://doi.org/10.1016/J.COLDREGIONS.2022.103487>
- Thapliyal A, Kimothi S, Taloor AK, Bisht MPS, Mehta P, Kothiyari GC (2023) Glacier retreat analysis in the context of climate change impact over the Satopanth (SPG) and Bhagirathi-Kharak (BKG) glaciers in the Mana basin of the Central Himalaya, India: A geospatial approach. *Geosyst Geoenviro* 2:100128. <https://doi.org/10.1016/j.geogeo.2022.100128>
- Vecchio LA, Lenzano MG, Durand M, Lannutti E, Bruce R, Lenzano L (2018a) Estimation of surface flow speed and ice surface temperature from optical satellite imagery at Viedma glacier, Argentina. *Glob Planet Change* 169:202–213. <https://doi.org/10.1016/j.gloplacha.2018.08.001>
- Vecchio LA, Lenzano MG, Durand M, Lannutti E, Bruce R, Lenzano L (2018b) Estimation of surface flow speed and ice surface temperature from optical satellite imagery at Viedma glacier, Argentina. *Glob Planet Change* 169:202–213. <https://doi.org/10.1016/j.gloplacha.2018.08.001>
- Vincent C, Ribstein P, Favier V, Wagnon P, Francou B, Le Meur E, Six D (2005) Glacier fluctuations in the Alps and in the tropical Andes. *Compt Rendus Geosci* 337:97–106. <https://doi.org/10.1016/J.CRTE.2004.08.010>
- Watson CS, Kargel JS, Shugar DH, Haritashya UK, Schiassi E, Furfaro R (2020) Mass loss from calving in Himalayan proglacial lakes. *Front Earth Sci* 7:1–19. <https://doi.org/10.3389/feart.2019.00342>
- Wu J, Pallé E, Guo H, Ding Y (2023) Long-term trends in albedo as seen from a lunar observatory. *Adv Sp Res* 72:2109–2117. <https://doi.org/10.1016/J.ASR.2023.06.028>
- Wu K, Liu S, Zhu Y, Liu Q, Jiang Z (2020) Dynamics of glacier surface velocity and ice thickness for maritime glaciers in the south-eastern Tibetan Plateau. *J Hydrol* 590:125527. <https://doi.org/10.1016/j.jhydrol.2020.125527>
- Wu Y, Wang N, He J, Jiang X (2015) Estimating mountain glacier surface temperatures from Landsat-ETM+ thermal infrared data: A case study of Qiyi glacier, China. *Remote Sens Environ* 163:286–295. <https://doi.org/10.1016/j.rse.2015.03.026>
- Wu Y, Wang N, Li Z, Chen A, Guo Z, Qie Y (2019) The effect of thermal radiation from surrounding terrain on glacier surface temperatures retrieved from remote sensing data: A case study from Qiyi Glacier, China. *Remote Sens Environ* 231:111267. <https://doi.org/10.1016/j.rse.2019.111267>
- Yalcin M, Polat N (2020) The impact of glacier surface temperature on the glacier retreat of Ağrı mountain. *J Indian Soc Remote Sens* 48:1433–1441. <https://doi.org/10.1007/s12524-020-01167-8>
- Yan W, Liu J, Zhang M, Hu L, Chen J (2017) Outburst flood forecasting by monitoring glacier-dammed lake using satellite images of Karakoram Mountains, China. *Quat Int* 453:24–36. <https://doi.org/10.1016/j.quaint.2017.03.019>
- Zemp M, Frey H, Gärtner-Roer I, Nussbaumer SU, Hoelzle M, Paul F, Haeberli W, Denzinger F, Ahlstrøm AP, Anderson B, Bajracharya S, Baroni C, Braun LN, Càceres BE, Casassa G, Cobos G, Dávila LR, Delgado Granados H, Demuth MN, Espizua L, Fischer A, Fujita K, Gadek B, Ghazanfar A, Hagen JO, Holmlund P, Karimi N, Li Z, Pelto M, Pitte P, Popovnin VV, Portocarrero CA, Prinz R, Sangewar CV, Severskiy I, Sigurdsson O, Soruco A, Usabaliev R, Vincent C (2015) Historically unprecedented global glacier decline in the early 21st century. *J Glaciol.* <https://doi.org/10.3189/2015JG15J017>
- Zhang Q, Zhang G (2017) Glacier elevation changes in the western nyainqentanglha range of the Tibetan Plateau as observed by TerraSAR-X/TanDEM-X images. *Remote Sens Lett* 8:1142–1151. <https://doi.org/10.1080/2150704X.2017.1362123>
- Zhang B, Wu Y, Lei L, Li J, Liu L, Chen D, Wang J (2013) Monitoring changes of snow cover, lake and vegetation phenology in Nam Co Lake Basin (Tibetan Plateau) using remote SENSING (2000–2009). *J Great Lakes Res* 39:224–233. <https://doi.org/10.1016/j.jglr.2013.03.009>
- Zhang YZ, Jiang XG, Wu H (2017) A generalized split-window algorithm for retrieving land surface temperature from GF-5 thermal infrared data. *Prog Electromagn Res Symp* 34:2766–2771. <https://doi.org/10.1109/PIERS.2017.8262224>
- Zhu Z, Woodcock CE (2014) Automated cloud, cloud shadow, and snow detection in multitemporal Landsat data: An algorithm designed specifically for monitoring land cover change. *Remote Sens Environ* 152:217–234. <https://doi.org/10.1016/j.rse.2014.06.012>

Springer Nature or its licensor (e.g. a society or other partner) holds exclusive rights to this article under a publishing agreement with the author(s) or other rightsholder(s); author self-archiving of the accepted manuscript version of this article is solely governed by the terms of such publishing agreement and applicable law.